LIBRARY
RESEARCH REPORTS DIVISION
NAVAL POSTGRADUATE SCHOOL
MONTEREY, CALIFORNIA 93940

NPS-67-83-003CR

NAVAL POSTGRADUATE SCHOOL

Monterey, California

CONTRACTOR REPORT

ELECTRICAL SPRAY MODIFICATION WITH VARIOUS FUELS IN A T56 COMBUSTOR

Avigdor Zajdman

March 1984

Approved for public release; distribution unlimited.

epared for:
val Postgraduate School
nterey, California 93943

NAVAL POSTGRADUATE SCHOOL
Monterey, California

Commodore R. H. Shumaker
Superintendent

D. A. Schrady
Provost

The work reported herein was carried out for the Naval Postgraduate School by Avigdor Zajdman under Contract Number N62271-82-M-1593. The work is part of a project sponsored by NAVAIR on Advanced Aircraft Propulsion Systems.

This report was prepared by:

UNCLASSIFIED

SECURITY CLASSIFICATION OF THIS PAGE *(When Data Entered)*

RMS **REPORT DOCUMENTATION PAGE**		READ INSTRUCTIONS BEFORE COMPLETING FORM
1. REPORT NUMBER NPS-67-83-003CR	2. GOVT ACCESSION NO.	3. RECIPIENT'S CATALOG NUMBER
4. TITLE *(and Subtitle)* Electrical Spray Modification with Various Fuels in a T56 Combustor		5. TYPE OF REPORT & PERIOD COVERED Contractor Report August 1982-September 1983 6. PERFORMING ORG. REPORT NUMBER
7. AUTHOR(s) Avigdor Zajdman		8. CONTRACT OR GRANT NUMBER(s) N62271-82-M-1593
9. PERFORMING ORGANIZATION NAME AND ADDRESS Naval Postgraduate School Monterey, California 93943		10. PROGRAM ELEMENT, PROJECT, TASK AREA & WORK UNIT NUMBERS
11. CONTROLLING OFFICE NAME AND ADDRESS Mr. George Derderian, Code AIR320B Naval Air Systems Command Washington DC 20361		12. REPORT DATE March 1984 13. NUMBER OF PAGES 61
14. MONITORING AGENCY NAME & ADDRESS *(if different from Controlling Office)* Naval Postgraduate School Monterey, California 93943		15. SECURITY CLASS. *(of this report)* Unclassified 15a. DECLASSIFICATION/DOWNGRADING SCHEDULE

16. DISTRIBUTION STATEMENT *(of this Report)*

Approved for public release; distribution unlimited.

17. DISTRIBUTION STATEMENT *(of the abstract entered in Block 20, if different from Report)*

18. SUPPLEMENTARY NOTES

19. KEY WORDS *(Continue on reverse side if necessary and identify by block number)*

Electrohydrodynamic spraying, electrostatic atomization, T56 combustor, electrical spray modification, Sauter Mean Diameter, alternative fuels.

20. ABSTRACT *(Continue on reverse side if necessary and identify by block number)*

The possibility of electrically altering the droplet size distribution and injection cone angle of gas turbine fuel injectors has been investigated. The work was carried out both in a combustor rig incorporating a T-56 combustor liner/nozzle and in a non-burning spray optical absorption apparatus into each of which a high voltage electrode could be introduced. Several electrode designs were investigated in an effort to minimize

DD FORM 1 JAN 73 1473 EDITION OF 1 NOV 65 IS OBSOLETE
S/N 0102-LF-014-6601

UNCLASSIFIED
SECURITY CLASSIFICATION OF THIS PAGE *(When Data Entered)*

20. Abstract continued.

flameholding and subsequent electrical short circuiting. Fuels investigated included JP-4, the design fuel, JET-A, JP-5, and Diesel Fuel Number 2.

Results of the optical experiments indicated reductions in the Sauter Mean Diameter of 7.7 percent. Results of the combustion experiments indicated increases in combustor efficiency of up to 3.6 percent for Diesel Fuel Number 2 and increases up to 0.6 percent for JP-4.

ABSTRACT

The possibility of electrically altering the droplet size distribution and injection cone angle of gas turbine fuel injectors has been investigated. The work was carried out both in a combustor rig incorporating a T-56 combustor liner/nozzle and in a non-burning spray optical absorption apparatus into each of which a high voltage electrode could be introduced. Several electrode designs were investigated in an effort to minimize flameholding and subsequent electrical short circuiting. Fuels investigated included JP-4, the design fuel, JET-A, JP-5, and Diesel Fuel Number 2.

Results of the optical experiments indicated reductions in the Sauter Mean Diameter of 7.7 percent. Results of the combustion experiments indicated increases in combustor efficiency of up to 3.6 percent for Diesel Fuel Number 2 and increases up to 0.6 percent for JP-4.

ACKNOWLEDGMENTS

The author wishes to express his deepest gratitude to the following individuals: Professors Oscar Biblarz and James Miller for providing the opportunity for the author to undertake this work during his sabbatical, and for their continuous support and participation as well as the many valuable discussions, Ted Dunton and Bob Besel for their willing helpfulness in providing every kind of technical support, Glenn Middleton for providing his superior technical skills with very fast time-response, Bob Sanders for his help with the quartz-insulated probe and the lending of measurement equipment, and LCDR John Mavroudis for participating in the initial successful phase while working on his Master of Science thesis. Last but not least, special thanks to LCDR Walter Manning, who colaborated in a major part of the combustion research, contributing new ideas, everlasting enthusiasm and persistence in the pursuit of meaningful results.

TABLE OF CONTENTS

1. INTRODUCTION 1

2. COMBUSTOR TEST RIG 4

2.1 AIRFLOW MEASUREMENT 4

2.2 FUEL FLOWRATE MEASUREMENT 7

2.3 TEMPERATURE MEASUREMENTS 9

2.4 HIGH VOLTAGE SUPPLY 12

2.5 HIGH VOLTAGE ELECTRODES 12

2.6 DATA ACQUISITION AND REDUCTION 22

3. OPTICAL SPRAY DIAGNOSTICS 26

3.2 RELATIVE SMD MEASUREMENT 26

4. COMBUSTION EXPERIMENTS 35

4.1 FUEL PROPERTIES 35

4.2 COMBUSTION TEST RESULTS 35

5. LIGHT ABSORPTION AND SCATTERING EXPERIMENTS 50

6. CONCLUSIONS 54

6.1 GENERAL 54

6.2 IMPROVED ELECTRODE DESIGN 54

6.3 INSULATED-NOZZLE COMBUSTION TESTS 54

6.4 SMD MEASUREMENT 56

7. SUMMARY 57

REFERENCES 58

APPENDIX A THE ELECTRIC INJECTOR A-1

APPENDIX A REFERENCES A-3

LIST OF FIGURES

1. T-56 Combustor Liner 3
2. Sharp-Edge Orifice for Airflow Measurement 5
3. Mass Flow Rate Calibration (4 Notch) 6
4. Turbine Flowmeter Calibration Curve 8
5. Thermocouple Array at Combustor Exit Plane 10
6. Probe Entry Locations 15
7. Flame Blow-off Designs (Top View) 16
8. Double-Insulated H.V. Probe with Flame Blow-off Control 17
9. Sealed-Pressurized, Quartz Insulated H.V. Probe 18
10. Exploded View of Ball-Joint Probe Mounted 20
11. Optical Alignment Fixture 21
12. Control and Data Acquisition Console 23
13. Schematic Diagram of the Combustion Apparatus 24
14. Combustor Details 25
15. Smoothed K Functions for Refractive Index n ≈ 1.5 28
16. Schematic Diagram of Optical Experimental Apparatus 30
17. Optical Bench 32
18. Optical Experimental Apparatus 33
19. Typical Probe Soot Deposition Pattern 38
20. Probe Detail Showing Internal Soot Deposits 39
21. Comparison of Thermal Combustion Efficiency Between JP-4 and DF-2, Probe at Zero Potential 41

22a. Temperature-Voltage Recording JET-A 42
22b. Temperature-Voltage Recording JP-5 43
22c. Temperature-Voltage Recording DF-2 44

23. Percent Transmission vs Applied Potential for a 10mm Gap in JET A . 51

24. Photograph of Light Absorption Experiment 52

25. Insulated Nozzle/Grounded Electrode 55

LIST OF TABLES

1. SUMMARY OF FUEL PROPERTIES 36

2. SUMMARY TEST RESULTS 45

1. INTRODUCTION

1.1 The shortage in petroleum has produced a trend in refining toward inclusion of heavier "fractions" in the fuel blends resulting in a wider range of viscosities, higher surface tension, and lower vapor pressure. The trend in increasing the aromatic content has developed consistently through the last decade [1]*, and the search for alternative fuel sources may well result in fuels of lower grade.

1.2 Changing to fuels of higher surface tension and viscosity would produce non-optimal sprays, both in pressure type atomizers [2] and in air blast type atomizers [3]. This result would be more pronounced in the latter type. Fuel sprays containing larger droplets of lower volatility exhibit longer evaporation and combustion time [4], resulting (for given combustor flow rates and geometry) in lower combustion efficiency, and higher soot production. This is especially important in high-performance aviation engines. Besides the deleterious effect on the overall propulsion efficiency, larger droplets may cause a significant reduction in the liner lifetime due to increases in radiative heat transfer [5]. Lower combustion efficiency also produces exhaust gases of more adverse environmental impact. It is therefore desirable to be able to incorporate in present-day combustors some means of modifying the fuel spray in order to compensate for the effects of higher viscosity and surface tension. This would enable the use of a wider variety of fuels for a given engine.

1.3 A simple yet potentially effective method of producing of finer liquid sprays is that of electrically charging the droplets. Electrical effects on droplets were first investigated by Rayleigh [6], and the applications have

* Numbers in brackets refer to references listed in the Bibliography.

achieved a growing interest in the spraying of paints, metals, and more recently in hydrocarbon fuels [7,8]. Mean droplet diameter reductions of 20 to 60 percent for fuels have been reported for cold sprays. Moreover, it has been postulated [9] that in a combustor, even if the droplets are not initially charged to the Rayleigh limit (at which they break into smaller drops), as they evaporate they eventually pass through that limit.

1.4 It appears, therefore, feasible to electrically modify fuel sprays in combustors in order to provide a desired control of droplet sizes and spray patterns. Accordingly an effort was initiated in 1980 in the Department of Aeronautics of the Naval Postgraduate School to investigate the viability of this concept. A combustor test rig, incorporating a modified T-56 gas turbine combustor liner, (Figure 1), was constructed [10]. Additionally, cold spray optical absorption and high speed photographic tests were performed [11] with encouraging results. A decrease in the relative amount of large droplets with a non-design (Diesel) fuel spray was detected under high electrical field influence [11], and high voltages were sustained by an electrode in the hostile environment of combustion gases [12]. A promising design has evolved in the construction of the high-voltage probe [13] which incorporates purging in the insulated portion of the electrode to achieve better flame blow-off control.

1.5 The objective of the present work was to continue this two-pronged effort while modifying the combustion test rig for higher productivity and more systematic data acquisition and reduction, and redesigning of the optical cold spray test setup to obtain more quantitative results. Along with these main goals, preferred electrode configurations were considered and alternative injection techniques were studied.

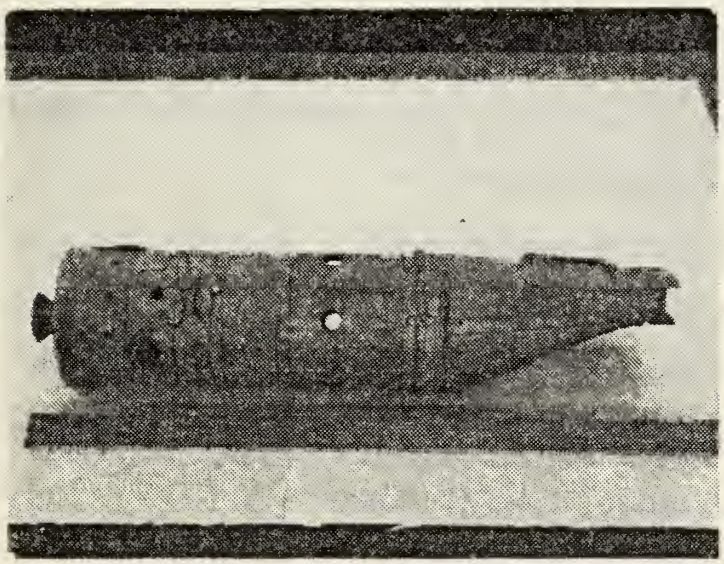

FIG. 1 T-56 COMBUSTOR LINER

2. COMBUSTOR TEST RIG

2.1 Airflow Measurement

2.1.1 In order to achieve more repeatable and reducible results it was necessary to measure and record the airflow to the combustor inlet with a well calibrated system. Orifice-type flow measurement was chosen as the fastest and most reliable method for this purpose. A standard 2.4 inch sharp-edge orifice (Figure 2) was manufactured from aluminum (the temperature range of the airflow was narrow enough to ensure accurate results with this metal) and mounted downstream of a flow straightener and a seven-foot long, eight-inch diameter pipe, and followed by an eight-inch diameter, five-foot exhaust pipe. Pressure taps were located one pipe diameter upstream from the orifice and one-half diameter downstream.

2.1.2 Calibration was performed by measuring the pressure drop across the orifice along with the pressure drop on a partially closed butterfly valve, upstream from the flow straightener. Air mass flow rate was calculated according to the procedure of Reference [14] using the values of flow coefficient K in Table 5, and Equation 2, Section 7 (ibid). The pressure drop across the butterfly valve, which was to serve as the "resistance" element, was measured first with a water manometer, and finally with a differential pressure transducer (Statham #12725, ± 1 psid). A simple linearized calibration formula was obtained:

$$W = 3000 \sqrt{\gamma h_w} \qquad (2.1)$$

where: W = airflow, in lb/hr

γ = specific weight of the flowing air in lb/ft^3

h_w = pressure drop across the valve, opened to the 4th notch, in inches of H_2O column height

Figure 3 is a plot of the calibration formula.

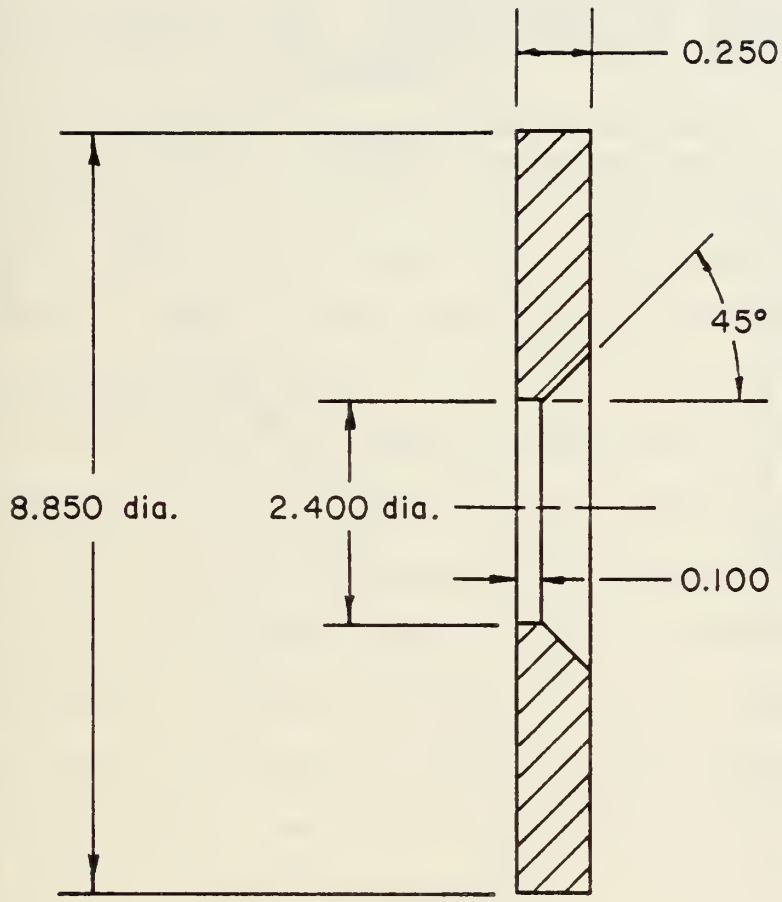

FIG. 2 SHARP-EDGE ORIFICE FOR AIRFLOW MEASUREMENT

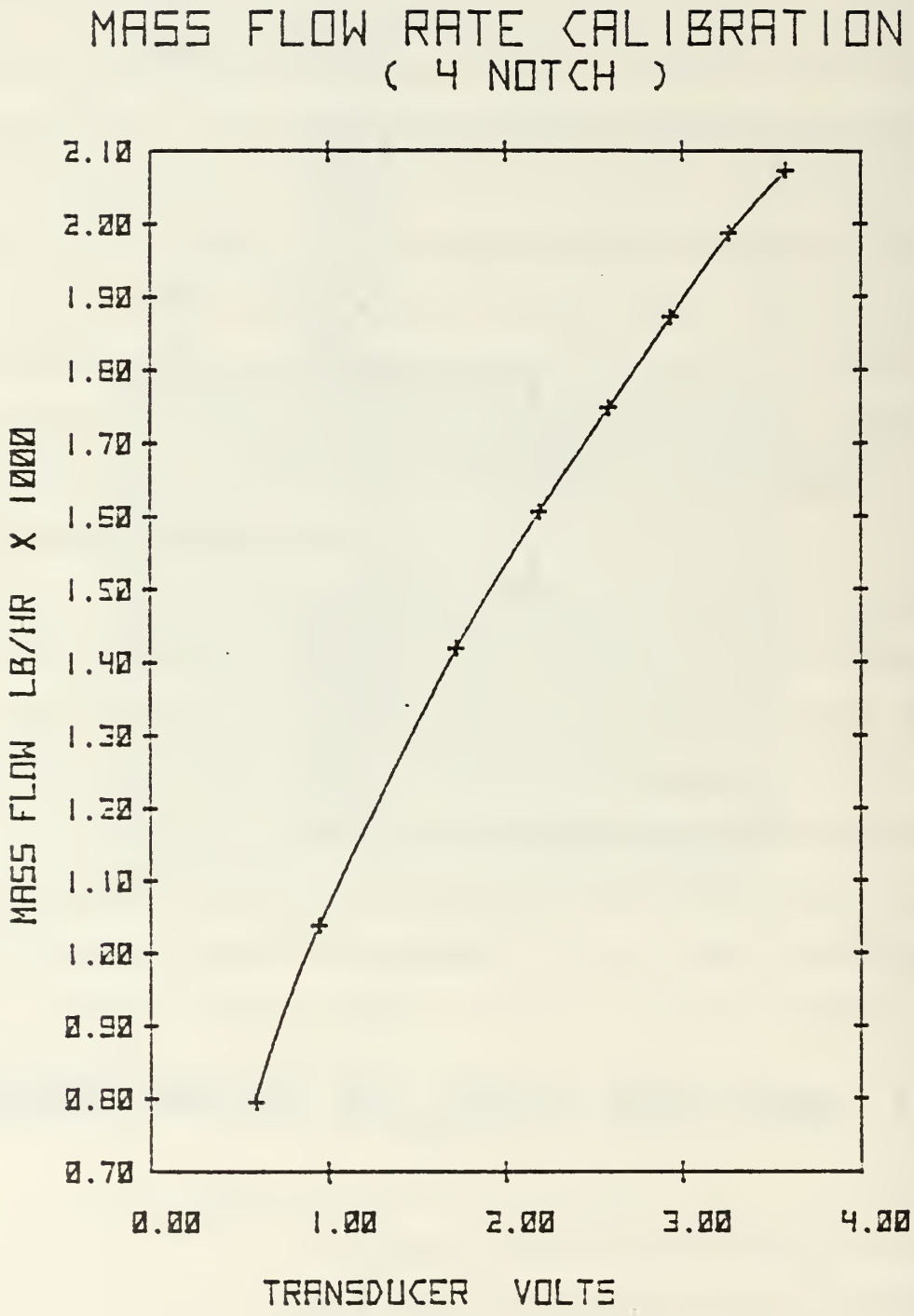

Figure 3. Mass Flow Rate Calibration (4 Notch)

For the differential pressure transducer this formula converts into:

$$W = 4000 \sqrt{\gamma \Delta V} \qquad (2.2)$$

where ΔV is the output of the transducer, in volts

This relation approximates the calibration curves of Reference [13] with an accuracy of 1.5 percent, indicating that the partially closed valve closely approximates an orifice. Airflow in this facility can be controlled, measured and recorded with an overall repeatability and accuracy better than 4 percent. Flow rates were observed to remain steady during test runs.

2.2 Fuel Flowrate Measurement

2.2.1 The fuel delivery system is comprised of a nitrogen-pressurized fuel container of 3-liter capacity along with nitrogen bottle with a pressure regulator and two solenoid-activated valves for fuel pressurization and for opening the fuel line to the combustor nozzle (the ARM and FIRE switches, respectively) [10]. Initially, due to the lack of a suitable flowmeter, average volumetric flows were obtained by dividing the fuel quantity for each test by the combustion time of the test (whenever ignition was immediate). Later, a turbine flowmeter was procured.

2.2.2 In order to verify the assumption of a constant fuel flowrate through the test, the turbine fuel flowmeter was installed. It consists of a Flow Technology Inc. turbine flowmeter Model FT-4-8 with RF-modulated pickoff providing a range from 0.06 to 3.0 GPM. This range covers, with suitable margins, the whole span of operation of a single T-56 nozzle. A pulse rate converter model PRC-408 from the same manufacturer provided a DC output for recording purposes. The flowmeter was calibrated by the manufacturer for the following viscosities: 0.85, 1.18, 7.32, and 16.12 cstks. A universal viscosity curve was generated and supplied by the manufacturer, its range covering the viscosities of most fuel blends (Figure 4).

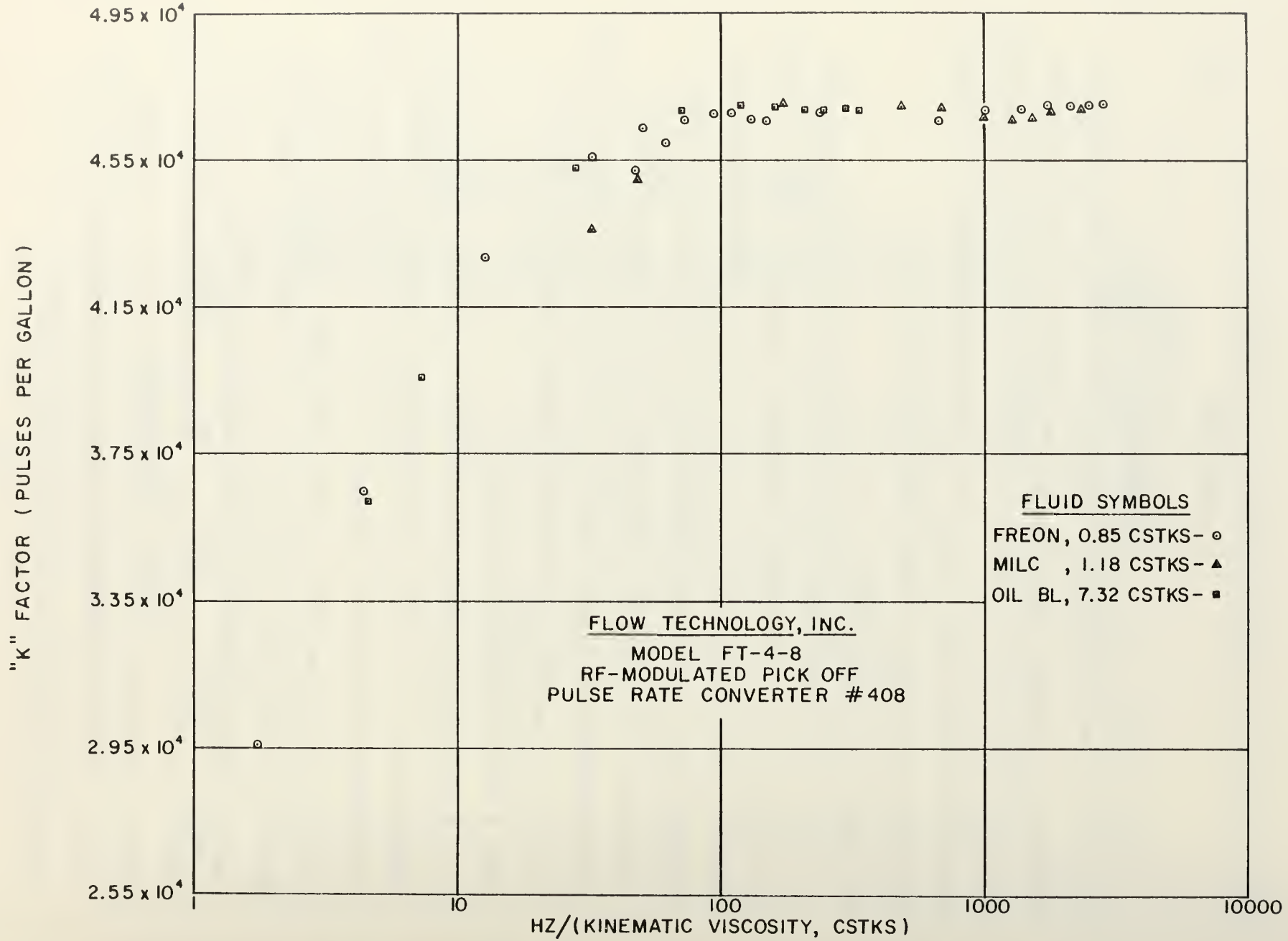

FIG. 4 TURBINE FLOWMETER CALIBRATION CURVE

2.2.3 After the turbine flowmeter was incorporated in the fuel delivery line, it was confirmed that:

- The fuel flowrate was steady for a given nitrogen pressure during the combustion tests (except for the fuel-exhaustion transient).
- The volumetric flowrate measurement was consistent with the flowmeter output to within 1 percent.

The first result is particularly significant, since for constant airflow (as reported in 2.1) there should be no appreciable change in combustor average exhaust temperature, unless there is a change in combustion efficiency.

2.2.4 The turbine flowmeter, however, proved to be susceptible to electrical noise, especially noise produced by sparking from the high voltage probe, during breakdown voltage tests. This noise caused damage to the pulse rate converter and repair was necessary. It was therefore necessary to avoid discharge or sparking tests when the flowmeter and pulse-rate-converter were on.

2.3 Temperature Measurements

2.3.1 During the initial phase of the project, through December '82, a single Chromel/Alumel thermocouple, (type "K"), was utilized to measure the combustor exhaust temperature. This thermocouple was of the stainless-steel shielded type. Later, 3 type "K" Inconel-shielded and ungrounded thermocouples were installed across the combustor exhaust to monitor the temperature profile and to enable an average temperature to be obtained, (through summing their outputs electrically). An additional Platinum/Platinum-Rhodium (type "R") thermocouple probe was installed and used for redundancy, since the "K" type thermocouples had the tendency to "burn-out" at the high temperatures. A photograph of the thermocouple installation is shown in Figure 5.

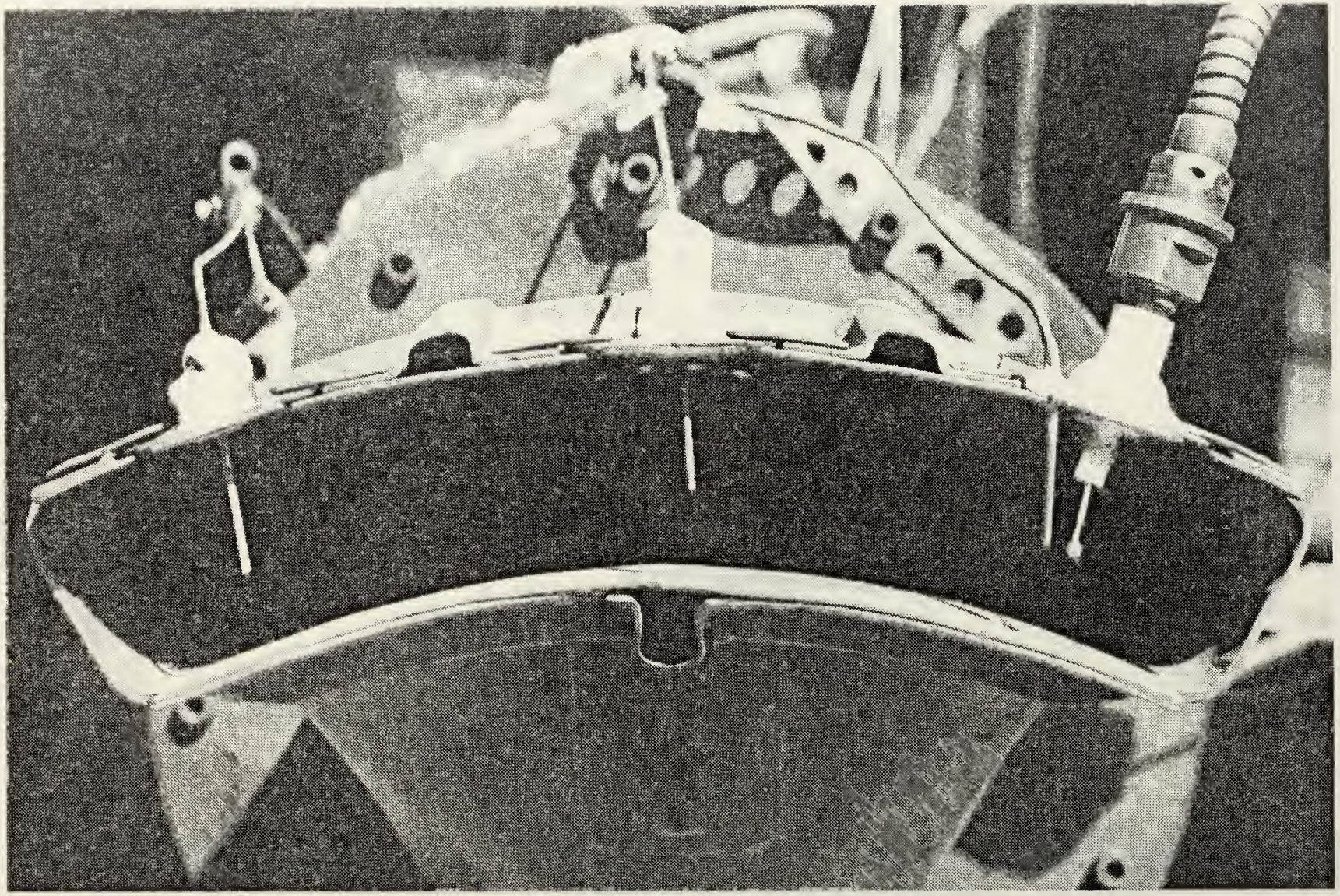

FIG. 5 THERMOCOUPLE ARRAY AT COMBUSTOR EXIT PLANE

2.3.2 The "sum-averaging" technique produced temperature measurements that were virtually noise-free, while each individual thermocouple indicated appreciable temperature fluctuation. The noise reduction was very dramatic, by a factor larger than $\sqrt{3}$, indicating that this "noise" was not an entirely random phenomenon, and that the temperature fluctuations at the various thermocouples were correlated. It was felt that those fluctuations were mostly caused by fluctuations in the fuel-spray spatial pattern (although the air and fuel flowrates remained constant). The sum of all three temperature measurements consistently cancelled out these fluctuations and essentially recorded constant energy flow through the combustor. Changes in the average exhaust temperature should be therefore interpreted as changes in the combustion efficiency as long as the air and fuel flowrates remain constant.

2.3.3 Results recorded with the 3 thermocouples reveal that in every instance when a rise in the central-thermocouple reading temperature was recorded an increase in average temperature was recorded as well. It is therefore justified to consider the positive results obtained with a single central thermocouple (2.3.1) as viable data.

2.3.4 The temperature measuring system was checked thoroughly and painstakingly for any possible noise generated by the discharge from the high voltage prove, and for the validity of the recorded temperature changes. Thermocouples were swapped, as well as their connections, leads and recorder channels. The high voltage was raised during cold flow (fuel and air) with intensive sparking up to the limit of ignition. The resulting noise was negligible and the temperature measurements through different thermocouples, lines and channels remained consistent.

2.3.5 Combustor inlet air temperature was monitored by a single "K" type thermocouple. No fuel temperature monitoring was performed since the fuel was

close to the ambient temperature which did not vary appreciably. References 11 and 12, however, indicate that the fuel to air temperature difference does affect spray characteristics.

2.3.6 The thermocouple outputs were recorded either directly or after processing through a digital thermometer with a linearized analog output, (Omega models 660 and DSS 650).

2.4 High Voltage Supply

2.4.1 A grounded-nozzle/positive-electrode configuration was used in the combustion experiments. A Sorensen 1030-20, high voltage power supply with a current limit of 20 mA was used in the initial phase, through December '82. It was replaced during the later phases of the investigation by Hipotronics Model 830-5/830B having a current limit of 5 mA. The high voltage was connected to the electrode through a coaxial cable with rounded-off external connections to prevent corona discharges.

2.4.2 The high voltage was sensed and recorded during the tests through a connection in parallel to the power-supply panel meter. Capacitors were employed to filter part of the noise induced by the moving-coil voltmeter. This arrangement proved suitable for low currents, but for the Hipotromics power supply the output was extremely noisy for currents above 1 mA. As a consequence, the voltage had to be monitored manually from the panel meter in these cases.

2.5 High Voltage Electrodes

2.5.1 There are two principal mechanisms through which droplet charging may be achieved:

2.5.1.1 Direct field emission into the liquid. This may be accomplished by producing local electrical fields on the order of 10^7 V/m. This necessitates the optimization of the electrical field at the nozzle tip,

(blunt external positive electrode, close in to the nozzle, in our case), or pre-charging the liquid before it enters the orifice, (Kelly's triode concept [9]).

2.5.1.2 Charging the droplets, after the spray is formed, through a corona discharge. In this case a high, ionizing electrical field is produced at the electrode tip and the droplets passing through the corona volume are electrically charged. A sharp-pointed electrode is best for this arrangement.

2.5.1.3 The first technique has some inherent advantages which result from the possibility of utilizing a grounded unshielded external electrode that could be even flame holding, with extremely low charging current (on the order of 100 μA for a typical combustor). The discharge currents for corona charging are inherently higher, necessitating power supplies of higher current capability.

2.5.2 As a result of cold-tests, it was found expedient at this stage to use a grounded-nozzle/hot electrode arrangement, resulting in fewer changes in the nozzle-combustor liner configuration. Alternate solutions will be discussed in Recommendations, Section 6. It should be noted here that maintaining an intense electrical field inside a combustor is extremely difficult due to the highly conductive combustion products [9], especially in the primary zone adjacent to the nozzle-electrode gap. The flame front is quite pliable and may engulf the high-voltage electrode, thus shielding the probe's electrical field from the fuel nozzle. Alternatively, it may cause prohibitively large leakage currents. In any case, the electrode must be both thermally and electrically insulated from the flame-front.

2.5.3 Two approaches to minimize the flameholding effect proved to be very effective.

2.5.3.1 Flame blow-off control. In the initial experiments by Logan [12] high voltage was sustained on the electrode during combustion tests with the electrode introduced through the crossover port and slanted upstream so as to create a 25 mm gap between the exposed tip of the electrode and the fuel nozzle. It was decided later [13] to introduce the electrode at a right angle to the flow at a distance of 25 mm from the nozzle plane in order to remove it further from the flamefront zone (Figure 6). Moreover, it was decided to try to minimize flameholding by the probe through the introduction of air or nitrogen purging through slots in the ceramic insulator near the electrode tip [13]. This technique is labeled "Circulation Control". Seven slot configurations were tested, they are depicted in Figure 7. Both air and nitrogen purging were investigated, the latter proving much more effective. The simplest yet most efficient flame blow-off slot arrangment was the dual-slot "E" configuration in Figure 7. For best results the slots had to be inclined slightly against the swirl in the air flow, produced by the slots in the backplate of the liner. In order to further insulate the electrode rod from the conductive flamefront, dual insulation was introduced [15] resulting in the probe configuration shown in Figure 8. With this probe it was possible to sustain near-clean-air-breakdown voltages during combustion for gap distances between 5 and 7.5 mm.

2.5.3.2 Sealed-off quartz insulation. Another approach to minimization of the flameholding effects was to construct a very thin sealed probe which is schematically shown in Figure 9. This configuration has the following advantages:

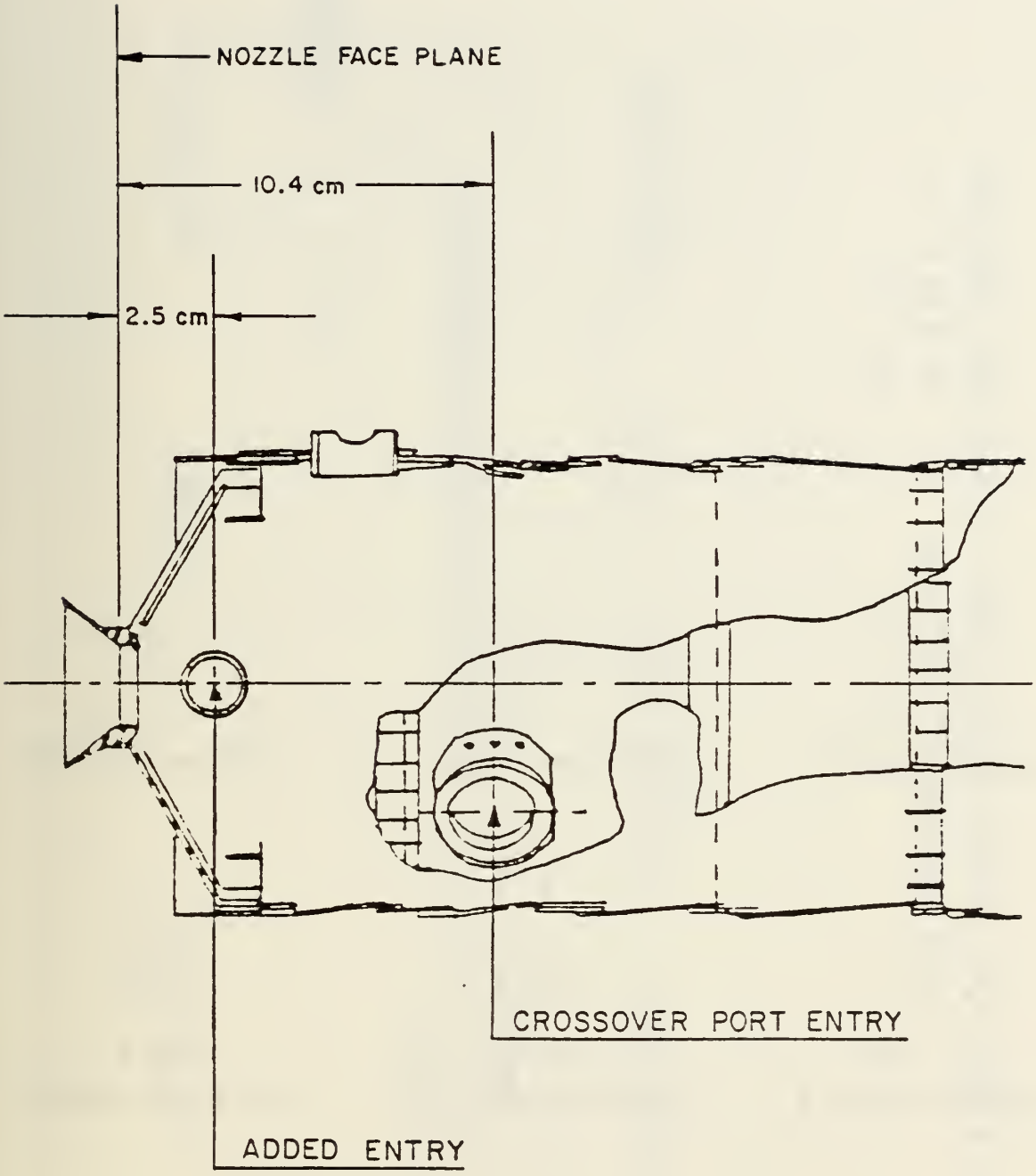

FIGURE 6
PROBE ENTRY LOCATIONS

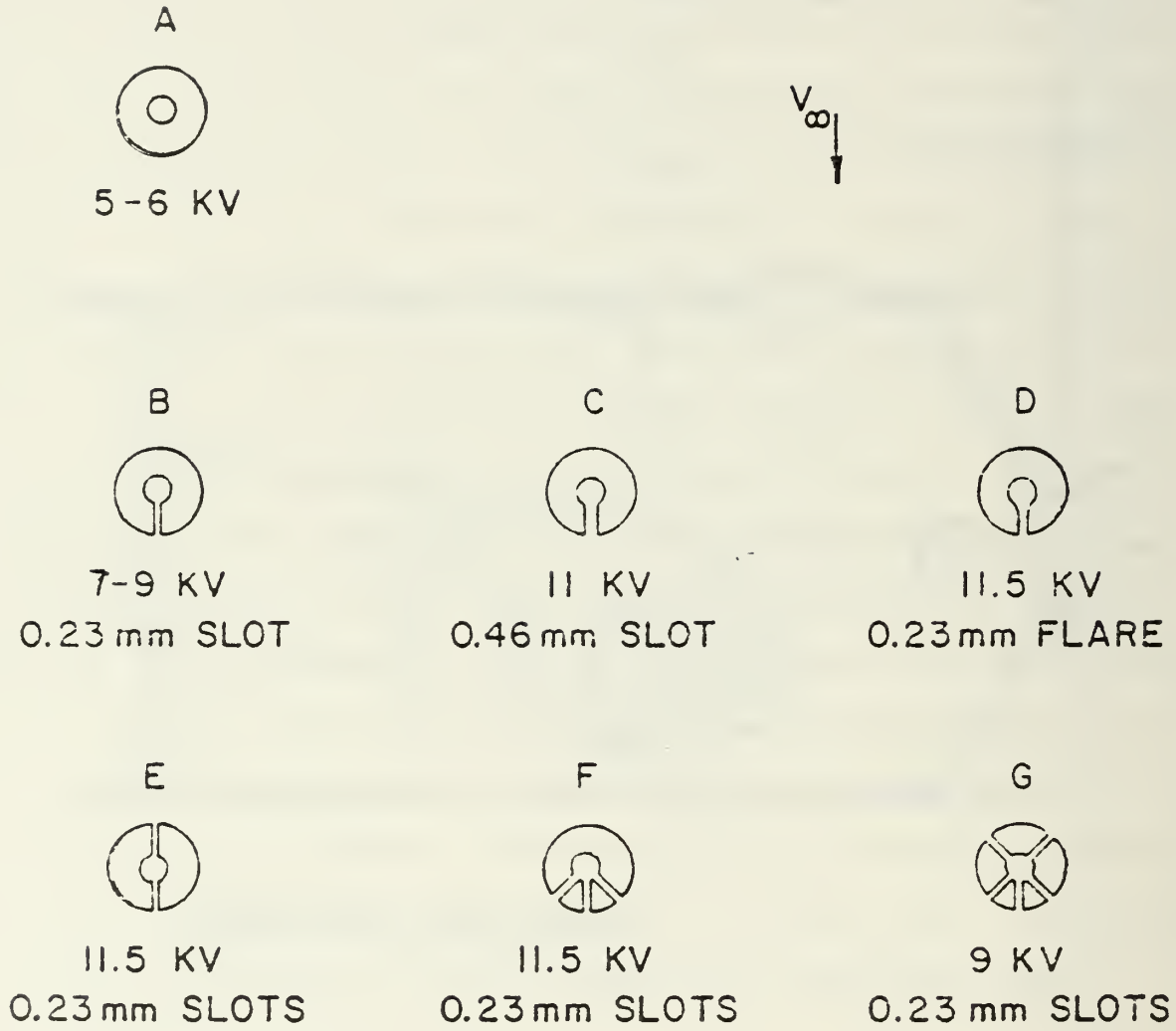

FIG. 7 FLAME BLOW-OFF DESIGNS
(TOP VIEWS)

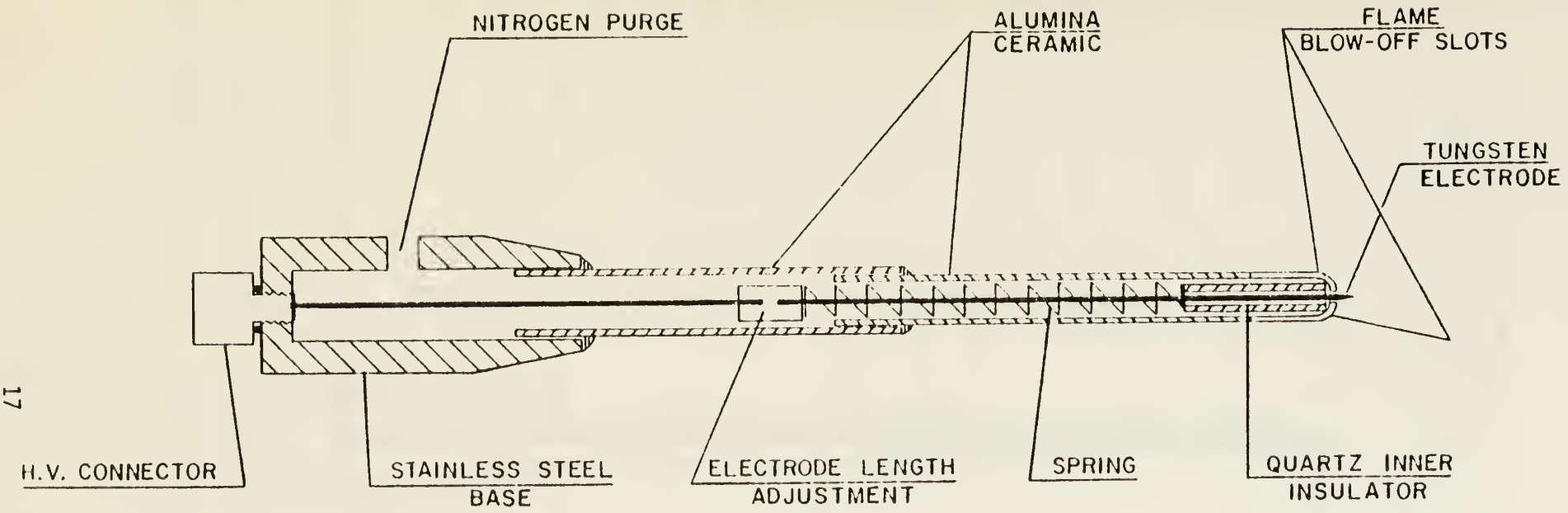

FIGURE 8
DOUBLE-INSULATED H.V. PROBE WITH FLAME BLOW-OFF CONTROL

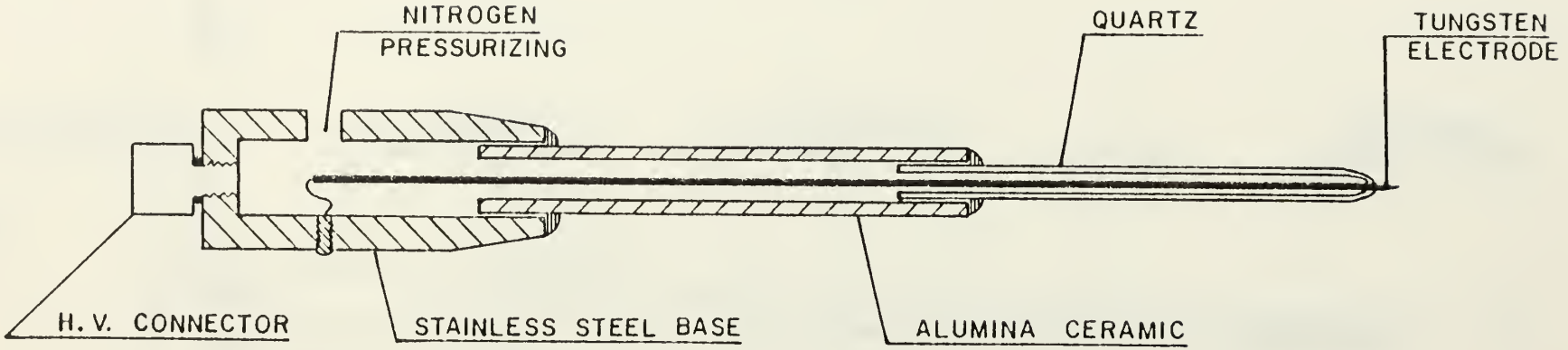

FIGURE 9
SEALED-PRESSURIZED, QUARTZ INSULATED H.V. PROBE

-It eliminates the need for nitrogen purging. (There is only a negligible amount of nitrogen needed for pressurizing and this could be eliminated with better quartz-metal seals.)

-The amount of maintenance is smaller, owing to the lack of fuel leakage into the insulated probe space.

-It could be used to construct bent probes to further eliminate flameholding.

This configuration proved to be as effective as the flame blow-off control, for short gap distances, ($\leq$ 10 mm). These results are discussed below.

2.5.4 Probe Mounting

The first ceramic-insulated probes were mounted rigidly on the combustor outer shell, (8" stainless steel pipe), [12,13]. It was realized however that an adjustable probe mount would be more suitable for extensive testing. A solution evolved (see [15]) resulting in a ball joint mounting. An exploded view of the mounting is shown in Figure 10. This was called the "4-degree-of-freedom" probe mounting; the ball joint provides two, while sliding the probe in and out and rotation along its axis provides two more. Sealing is provided by the ball joint itself and by an "O-ring" squeezed around the ceramic insulator on the open air end of the probe. An external calibrated scale provided fast and easy adjustment of the electrode-nozzle gap distance to within $\pm$ 0.5 mm, while a specially constructed optical insert, (right-angle finder-telescope), permitted precision alignment of the electrode tip on the combustor centerline (Figure 11). With this arrangement a whole range of gap distances, from 5 mm to 35 mm, could be scanned and the flame blow-off slots could be empirically aligned with the local flow direction, thus compensating for the swirl in the flow.

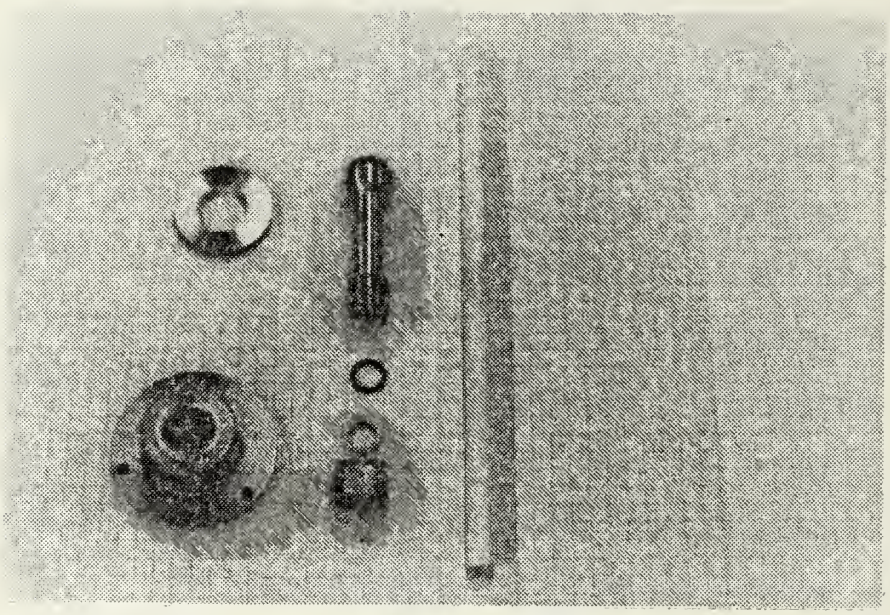

FIG. 10 EXPLODED VIEW OF BALL-JOINT PROBE MOUNT

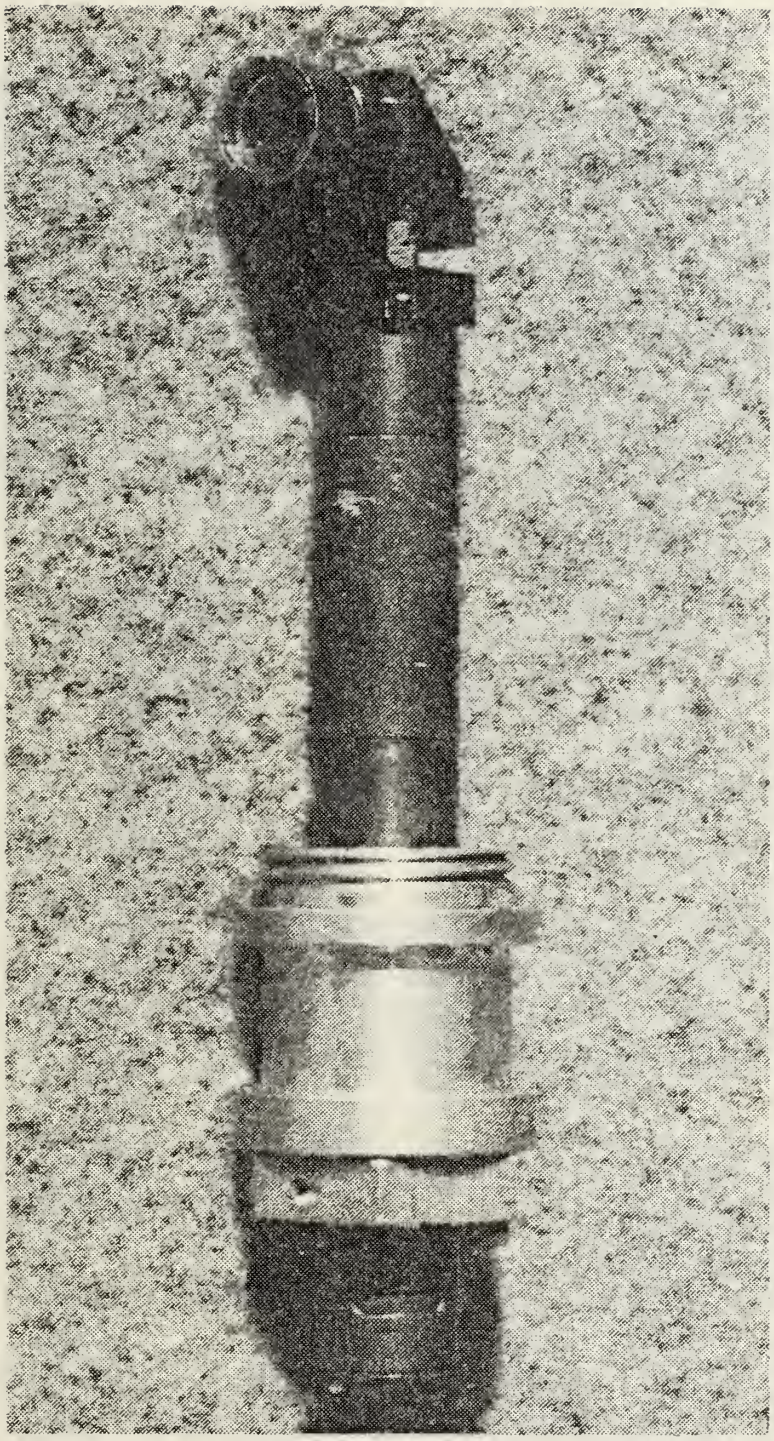

FIG. 11 OPTICAL ALIGNMENT FIXTURE

2.5.5 Probe Insulation

The principal insulation for the probes was high-density alumina ceramic tubes (Coors Cast Alumina Tubes AD-998). Care was taken so that the dielectric strength at the joint and liner port exceeded the electrical breakdown requirement for the largest electrode-nozzle gap, (V>22 kV). The insulation also should have provided excellent high-temperature protection for the electrode rod but electrical insulation at the high-temperature of operation was not verified. In the purged probe there was "built-in" film-cooling, but even in the quartz-sealed probe there was no evidence of electrode oxidation or failure. This is quite remarkable, since the probe is actually immersed in the primary zone, with temperatures of approximately 2500°K.

2.5.6 Electrode Material

Tungsten was used in the high voltage probes, due to its high melting temperature. Stainless steel might have been used as well in the purged probes, due to the film cooling. Electrode rods could be easily exchanged in the purged probe, (Figure 9), thus enabling investigation of both sharp-pointed and blunt tips.

2.6 Data Acquisition and Reduction

Four dual-channel strip-chart recorders, capable of better than one percent full scale resolution provided channels for combustor exhaust temperature, (either directly from thermocouples or through linearized-analog outputs of digital thermometers), air flowrate, fuel flowrate and high voltage. Two HP-41C calculator programs were written: "AF" (by J. Mavroudis) and "ER" (by W. Manning) for equivalence ratio calculation. The Control, Operation and Data Acquisition console is shown in Figure 12. The combustor test rig is shown diagramatically in Figure 13. A photograph of the combustor is shown in Figure 14.

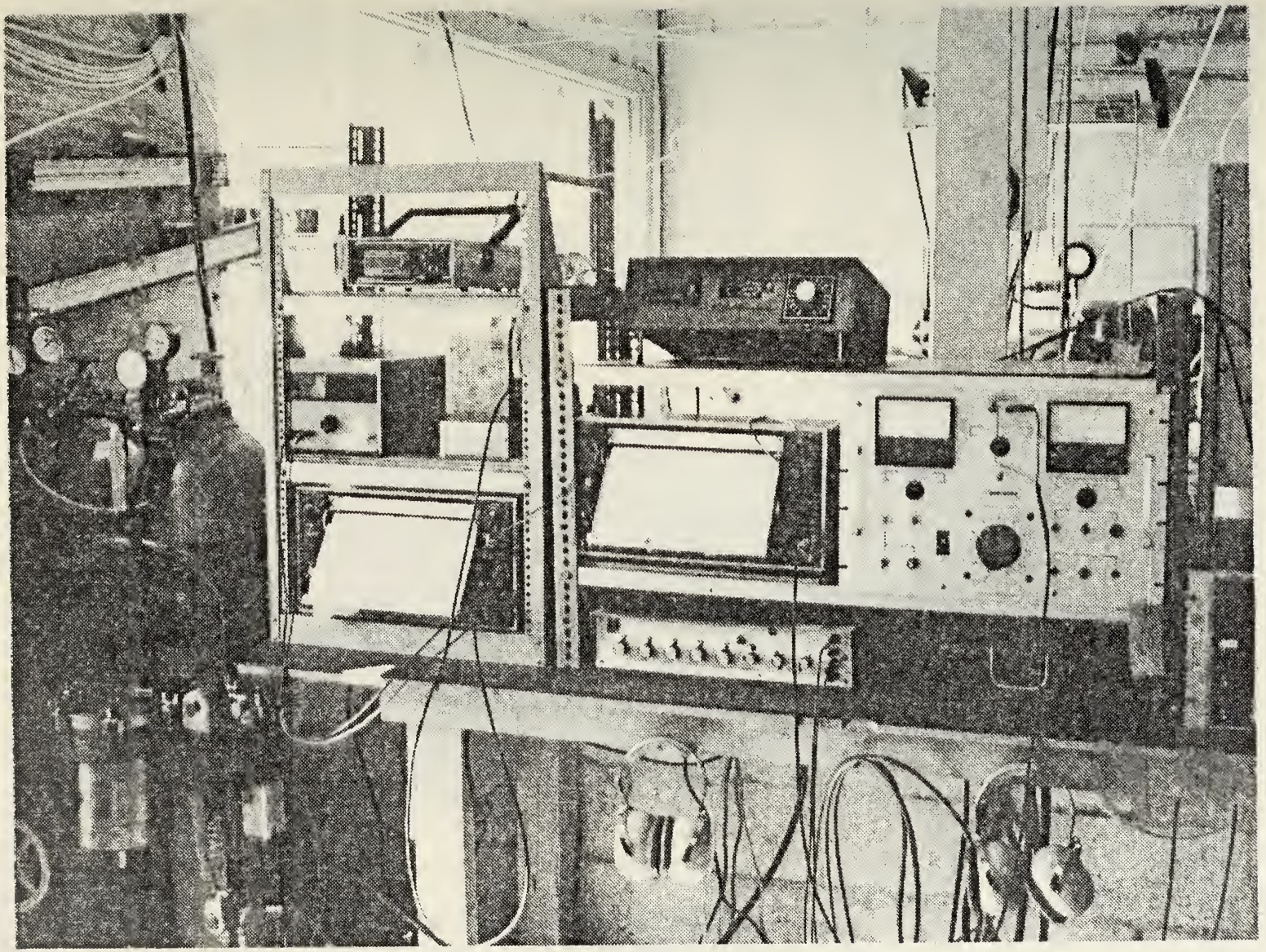

FIG. 12 CONTROL AND DATA ACQUISITION CONSOLE

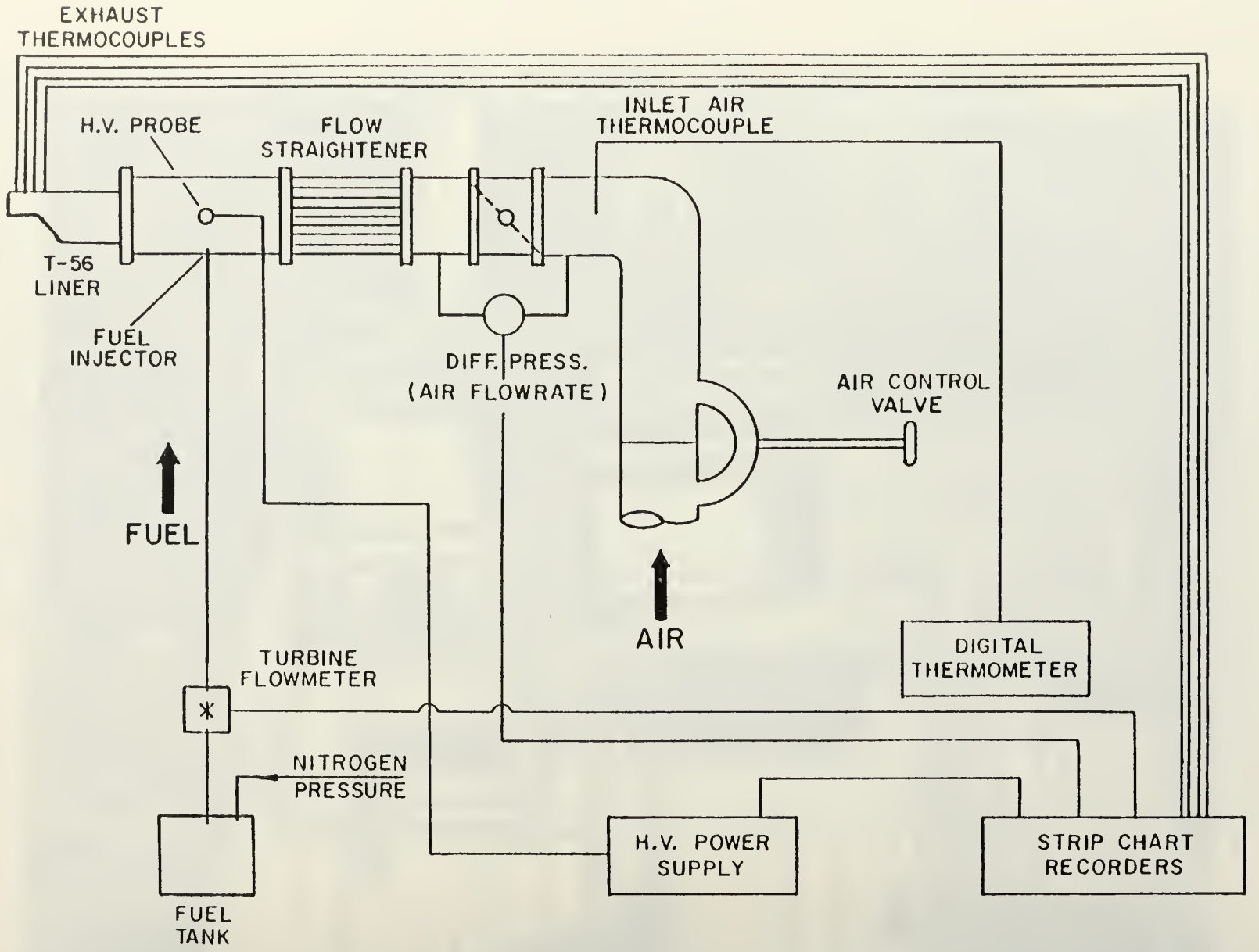

FIGURE 13
SCHEMATIC DIAGRAM OF THE COMBUSTION APPARATUS

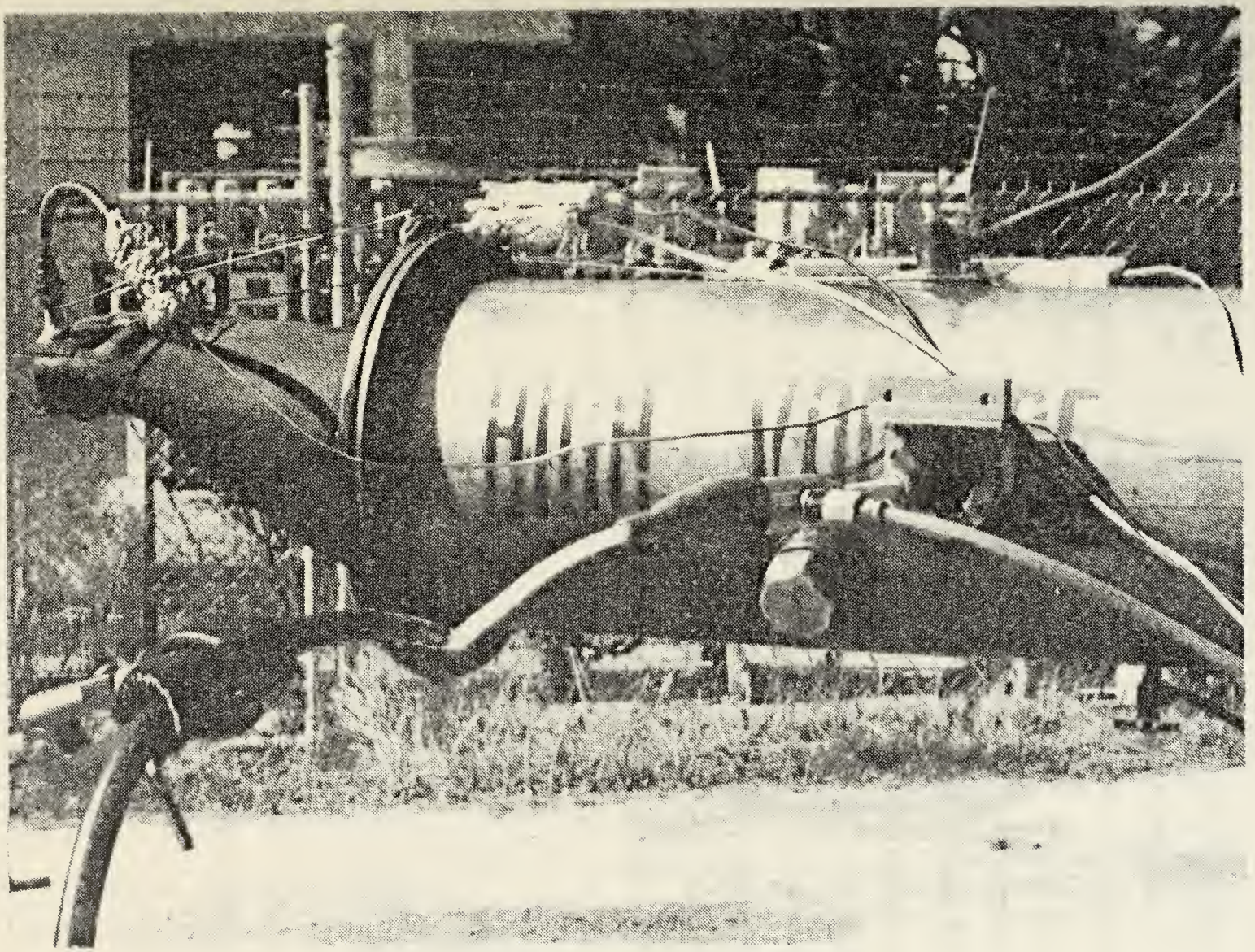

FIG. 14 COMBUSTOR DETAILS

3. OPTICAL SPRAY DIAGNOSTICS

3.1 Droplet size measurements are essential in this kind of research in order to guide electrode configuration design and to correlate the combustion test results to the actual spray changes obtained through electrical modification. Of the methods that exist for droplet size measurements, optical methods are considered the least intrusive. Optical methods vary in accuracy and complexity, from the measurement of Sauter Mean Diameter, (SMD or D_{32} - the "ratio of volume to surface" diameter), (Dobbins et al., [16], Rizkalla and Lefebvre [17]), to SMD and distribution width (via wavelength measurement), (Cashdollar et al., [18]), to particle size and velocity distribution function measurement (two-beam interferometry), (Bachelo et al., [19]). The latter method is very expensive (on the order of $100,000.00 for equipment alone). A three-wavelength measurement was considered initially, but a submillimeter-wavelength source, needed to account for the largest droplet size, (~ 1 mm), was not readily available. Within the budget and timeframe constraints, a simple adaptation of the SMD measurement experimental setup was designed and constructed.

3.2 Relative SMD Measurement

3.2.1 Theoretical Background. The transmission of light(T) passing through a spray of a path length ℓ, having a Sauter Mean Diameter D_{32}, and a volume concentration C_v is given by [16]:

$$T = \exp\left(-\frac{3}{2}\,\frac{\bar{K}}{D_{32}}\,\ell C_v\right) \qquad (3.1)$$

where $\overline{K}$ is the mean total Mie - scattering coefficient for the droplet size distribution of the spray. The coefficient $\overline{K}$ is dependent on the wavelength of light λ, droplet size D, and index of refraction n. All these parameters combine into a single governing "normalized size parameter", ρ (also described as the phase shift parameter [20]):

$$\rho = 2\alpha(n - 1) \tag{3.2}$$

where:

$$\alpha = \pi D/\lambda$$

The index of refraction, n, for the fuels utilized in the present work, may be assumed to be within the limits: $1.3 < n < 1.5$ (these are the extreme limits for various hydrocarbon fuel fractions). The behavior of $\overline{K}$ as a function of α for $n = 1.5$ is given by Penndorf [21], in Figure 15 from which it can be seen that the value of $\overline{K}$ converges for very large values of α to a constant value of nearly 2.0. This is consistent with the diffraction theory of light [22], since the term:

$$\frac{3}{2}\,\frac{C_v}{D_{32}}$$

in the transmission law (3.1) represents the total projected area of the droplets, and for droplets much smaller than the probe beam diameter the scattering cross section is twice the projected area. For our range of interest, $D>20$ μm, $\lambda = 0.6328$ μm (He-Ne laser), $\alpha > 100$, and $\overline{K}$ should be very close to 2.0 and virtually independent of D_{32}. Penndorf's approximation [21] for extreme values of K is given by:

$$K_{max} = 2 + \frac{4}{\rho_{max}} + \frac{4}{\rho_{max}^2} + \frac{29M}{\rho_{max}} - \frac{51M}{\rho_{max}^2}$$

$$K_{min} = 2 - \frac{4}{\rho_{min}} + \frac{4}{\rho_{min}^2} + \frac{8.01M}{\rho_{min}} - \frac{27.3M}{\rho_{min}^2} \tag{3.3}$$

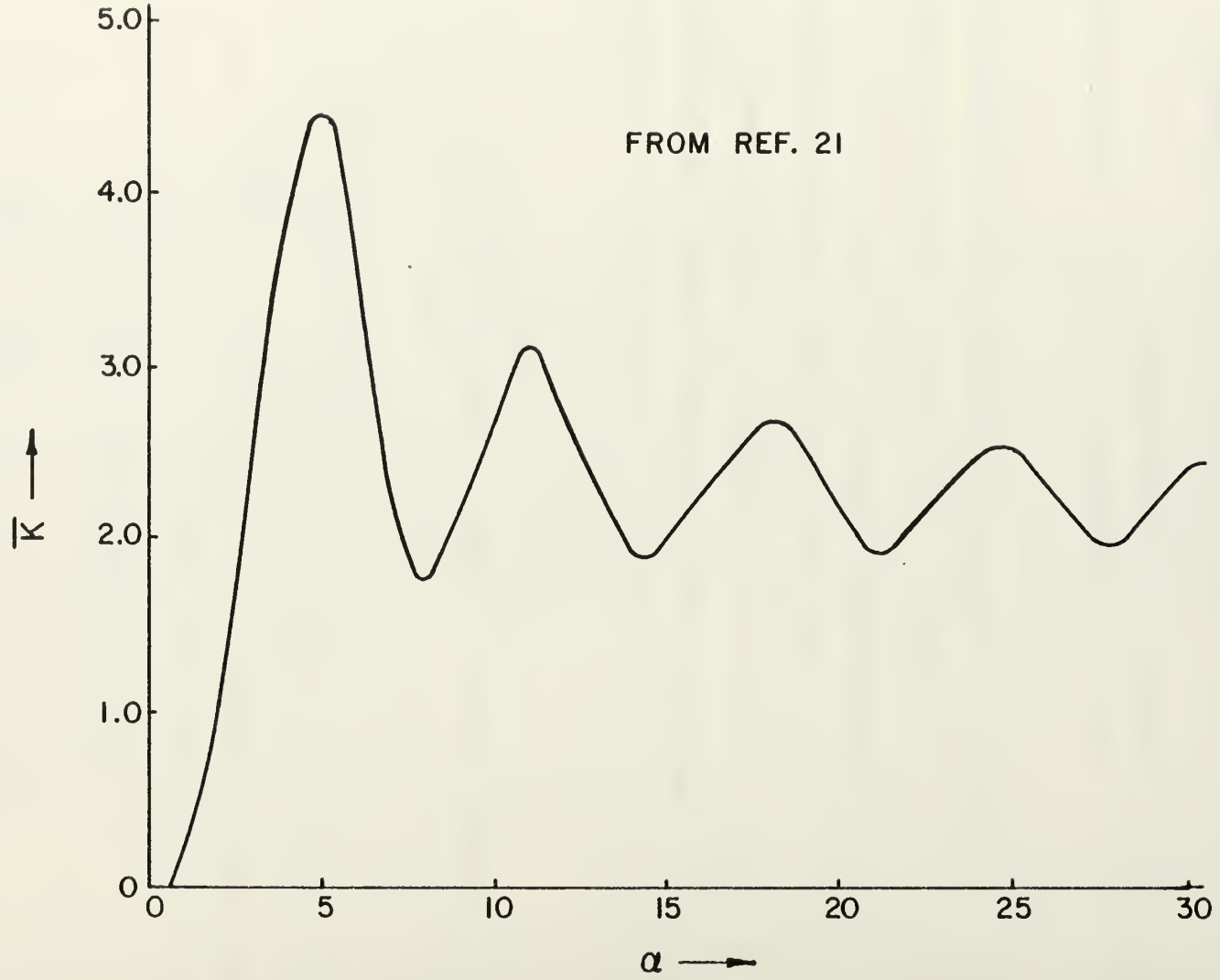

FIG. 15 SMOOTHED K FUNCTIONS FOR REFRACTIVE INDEX $n \approx 1.5$

where M is the Lorentz - Lorenz term:

$$M = (n^2 - 1)/(n^2 + 2)$$

Averaging minimum and maximum values, to evaluate an approximate value of $\overline{K}$ for $1.3 < n < 1.5$ yields:

$$\overline{K} = 2.04 \pm 0.04 \qquad (3.4)$$

(the error limits are due to the uncertainty in n, which is constant for each fuel, yielding a constant value of $\overline{K}$). For constant fuel flowrates, ℓ = const., C_v = constand it is therefore possible to obtain the relative change in D_{32} with electrohydrodynamic spray enhancement:

$$\frac{\ell n\ T(V = 0)}{\ell n\ T(V \neq 0)} = \frac{D_{32}\ (V \neq 0)}{D_{32}\ (V = 0)} \qquad (3.5)$$

3.2.2 Experimental Apparatus

3.2.2.1 The experimental setup for the relative SMD measurement is shown schematically in Figure 16. The 5 mW HeNe laser beam, (Hughes Model 3305H) is chopped by a calibrated mechanical chopper, (Laser Precision Corp. CTX-534), and split by a variable density beam splitter, (Jodon VBA-200), into the probe and reference beams. The reference beam is attenuated, (by reflection off an optical flat and a ~ 0.3/0.7 beam splitter), and focused through a 50 μm pinhole into a SGD-100A, (EG&G), photodiode. The probe beam is expanded by a X10 beam expander, passed through the spray, and focused by an f = 60 cm lens, through a 100 μm pinhole onto a similar photodiode. The probe signal is detected by a PAR 121 lock-in amplifier, the unperturbed signal from the first photodiode serving as reference. The output, representing the transmission T, (Equation (3.1)), is recorded, along with a sample of the high voltage on an x-y recorder providing a continuous graph of transmission vs. voltage. The natural log of T can be calculated for

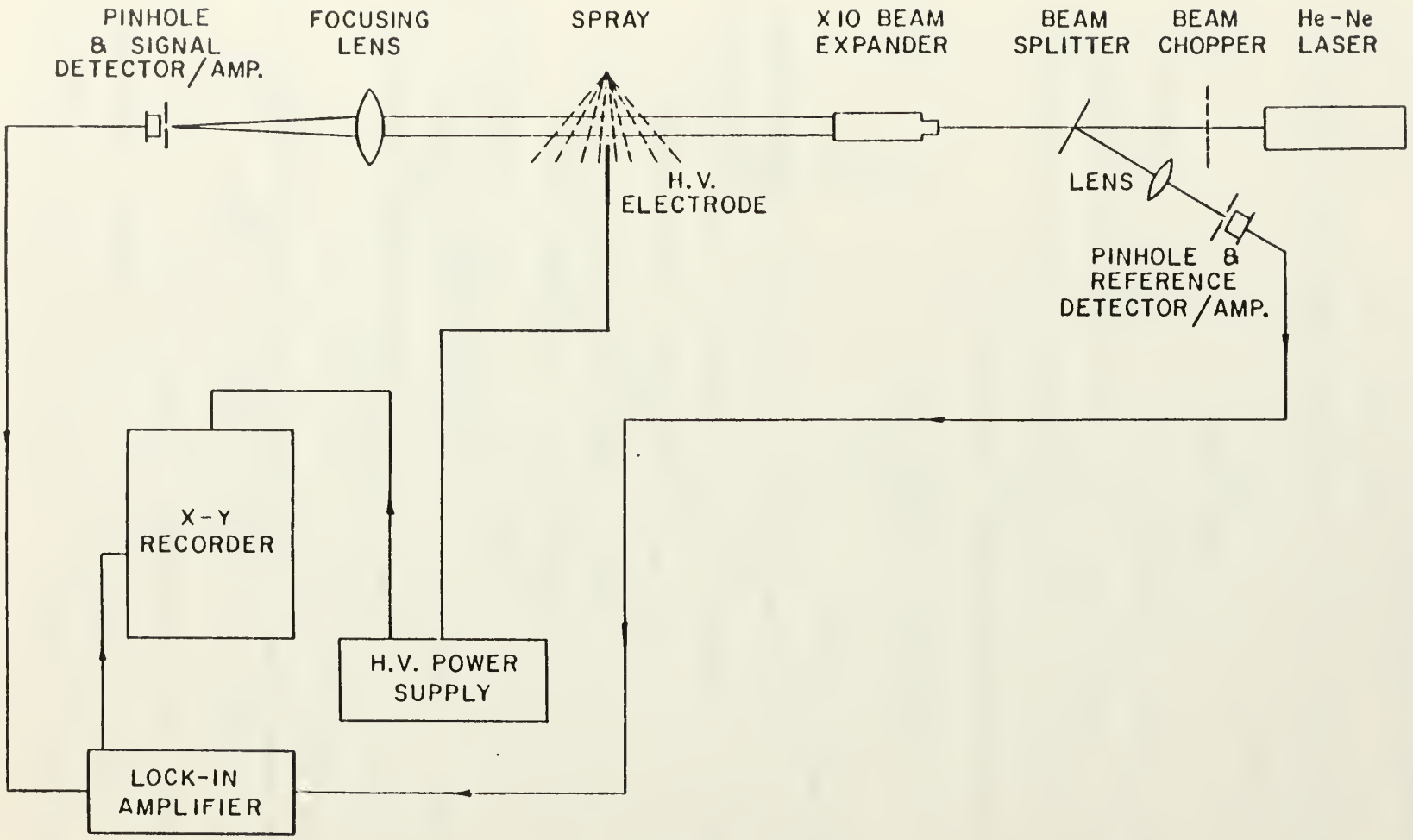

FIGURE 16
SCHEMATIC DIAGRAM OF OPTICAL EXPERIMENTAL APPARATUS

any V, providing the dependance of D_{32} and V. These values are adjusted for the changes in C_V and ℓ caused by the slight cone angle expansion of the charged spray. Generally, C_V decreases inversely proportional to ℓ^2.

3.2.2.2 The standard T-56 fuel nozzle and the electrode are mounted on a vertical optical bench, on electrically insulated sliding mounts, enabling the movement of the electrode and nozzle with repsect to each other and to the probe beam, (see Figure 17). Nitrogen is purged through the air shroud of the nozzle to improve spray confinement and to deter ignition in the case of sparking betweeen the nozzle and the electrode. The spray is directed vertically downwards through a funnel mounted in the tabletop, into a covered, grounded pan. In this manner lab space, table and floor contamination by the fuel spray is almost entirely eliminated. Either the electrode or the nozzle may be grounded or connected to the reversible polarity high-voltage supply. High voltage resistors having a resistance of 70 MΩ may be connected in line with the "hot" electrode to minimize the current in case of breakdown.

3.2.2.3 The experimental arrangement, shown also in Figure 18, ensures a very high, (better than 200), signal-to-noise ratio. It also produces an accurate measurement of the transmission, since:

-the beam diameter is at least 10 times greater than the largest droplet size;

-only the diffraction-limited (unscattered) part of the beam is measured by the photodiode, and only a negligible percentage of the radiation scattered by even the largest droplets is transmitted by the pinhole.

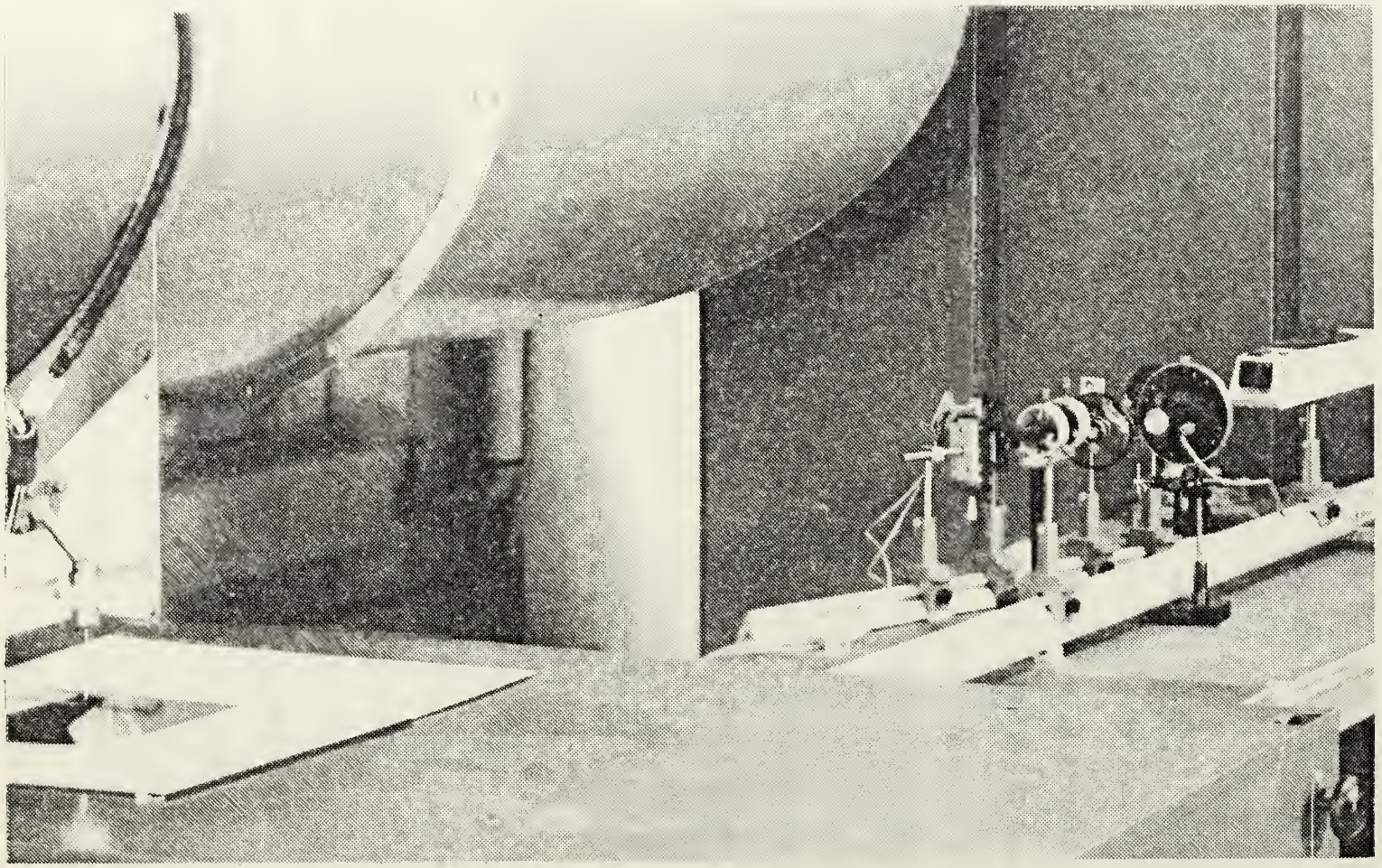

FIG. 17 OPTICAL BENCH

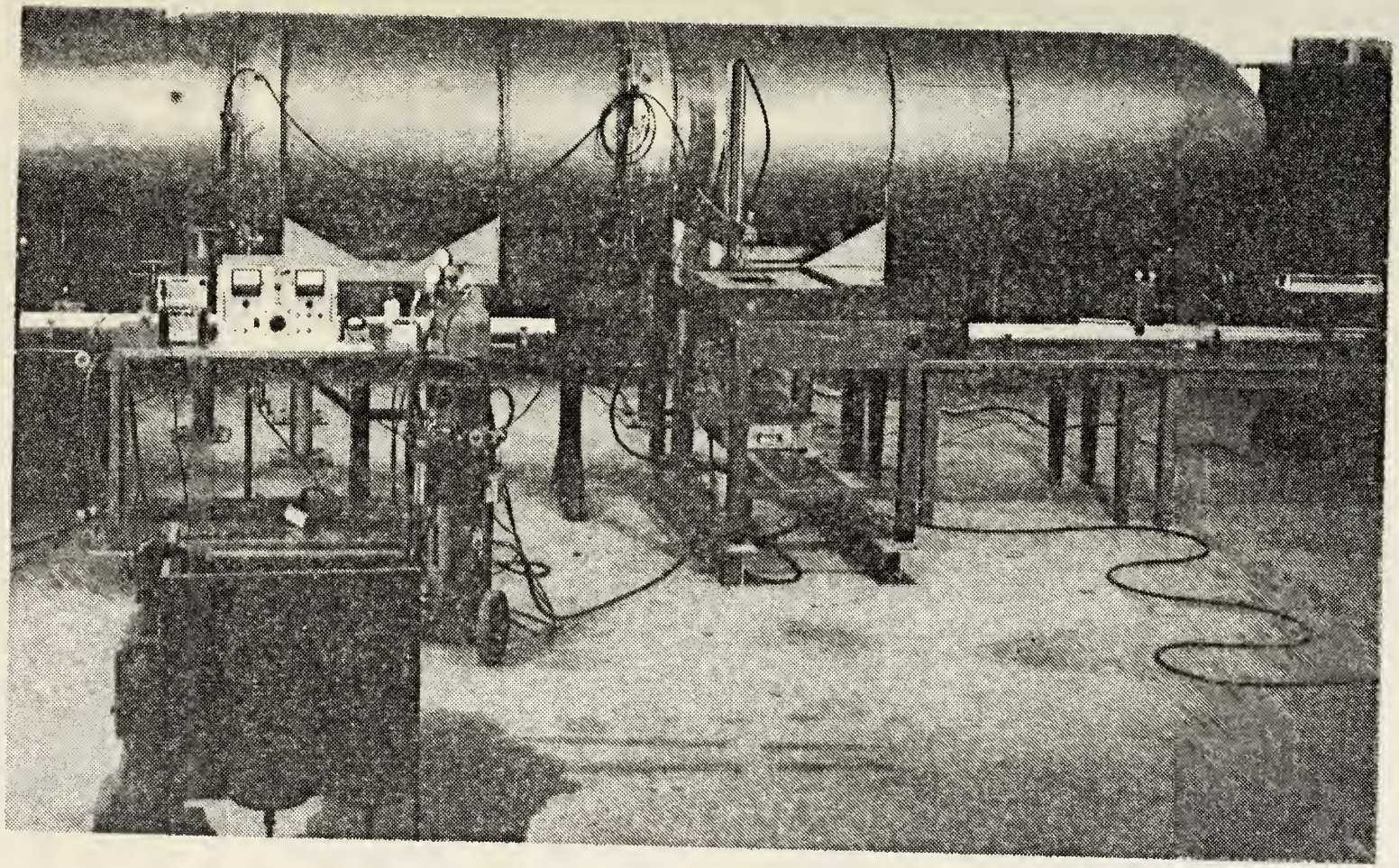

FIG. 18 OPTICAL EXPERIMENTAL APPARATUS

It was possible to operate this setup with the vibration generated by a 300 HP running air compressor at a 5 m distance, with only 2 percent degradation in the overall performance.

3.2.3 Absolute SMD Measurement

Dobbins et al., [16] and Roberts and Webb [23] have shown that, assuming droplet size distribution according to an upper-limit-distribution function (ULDF), the illumination profile of the scattered light versus reduced angle, $(\pi D_{32}/\lambda)\theta$, follows a nearly universal mean theoretical curve for a wide range of size distribution parameters. This curve is given in both [16] and [23] and may be utilized for SMD calculations from angular light distribution measurements in the far field. More recently, it has been shown (Reference 24), that a fairly good approximation to a polydisperse spray light scattering pattern representative of fuel sprays where $\alpha\theta<3$ is given by:

$$\frac{I(\theta)}{I(0)} = \exp\left[-(0.57\ \alpha\ \theta)^2\right] \qquad (3.6)$$

where $\alpha = \frac{\pi D_{32}}{\lambda}$

θ = scattering angle

Given any two $I(\theta)$ values, D_{32} may be readily calculated. The experimental setup (Figure 17) could be easily adapted for $I(\theta)$ measurements. A larger focusing lens and pinhole were utilized, to capture enough of the scattered light and ensure the linearity of the measurement. The chopper frequency was raised to 4 kHz to provide some "freezing" of the droplet motion. Micrometric screws with 0.01 mm resolution were used to move the pinhole along the focal plane. Three points of $I(\theta)$ could be measured during a typical short run. A better arrangement is suggested in the Recommendations, Section 6.

4. COMBUSTION EXPERIMENTS

4.1 Fuel Properties

Both commercially available and military fuels were used in this program. JP-4 is the design fuel for T-56 combustor, and is a high grade fuel of high H/C, low viscosity and surface tension. JET-A and JP-5 are also high quality jet propulsion fuels, although of greater viscosity and surface tension. Diesel fuel has the lowest value of H/C and is representative of high surface tension, high viscosity fuels. These chartacteristics of Diesel fuel should result in coarser sprays, less efficient combustion, higher luminosity flame and more soot at the exhaust. The major properties of the fuels used are listed in Table 4.1. It should be noted that some fuel samples from different batches had different compositions and characteristics.

4.2 Combustion Tests Results

4.2.1 General

With the fuel flowrate constant during each run, the air flowrate was adjusted for each test. It was possible to perform 2 to 3 tests during a typical 3 to 4.5 minute run, each test consisting of a different equivalence ratio.

With all the improvements incorporated in the combustor test rig it was possible to average about 16 tests per day although as many as 27 tests were actually performed on a single day.

In all 385 individual tests were run. Of these, 81 tests had to be discarded due to thermocouple burnout. An additional 71 tests were discarded in the period of April 26 through May 9, 1983, due to poor nozzle performance resulting from a defective orifice. The balance of 233 tests were deemed acceptable for data reduction.

TABLE 1

Summary of Fuel Properties

Fuel	Hydrogen(3) wt %	Aromatics(3) volume %	Density(3) kg/m^3	Kinematic(4) viscosity cst, at 16°C	Surface(5) Tension N/m $X10^{-3}$, at 20°C	Net Heat(3) of Combustion MJ/kg
JP-4(2)	14.1	14.1	755	1.03	23.5	43.4
JP-5(1)	13.3	22.7	827	2.2	29*	42.9
JET-A(2)	13.4	18.9	822	2.1	25.6	43.0
DF-2(2)	12.3	48.5	870	8	28.8	42.4
JET-A(1)	13.4	22.3	827	2.1	31.3*	43.0
DF-2(1)	12.7	67.0	861.5	7.5	42.4*	42.6

(1) Batch used through December 1982

(2) Batch used January - September 1983

(3) Analysis performed by Energy Management Laboratory, Wright-Patterson AFB, Reference (10)

(4) Data from above source, adjusted for temperature

(5) By capillary tests

* From [13]

4.2.2 High Voltage Probes Performance

It is worth noting that the probe design, although simple, was not straightforward and, for example, thinner probes were not always more effective in the reduction of the flameholding effect than thicker ones.

Much trial-and-error testing based on soot deposition on the probe was needed to align the slots properly with the flow and to optimize the nitrogen purging rate at each probe position (see Figure 19).

Fuel leakage into the insulated probe housing posed another problem. Fuel collected within the probe housing would undergo thermal decomposition and form conductive deposit on the electrode rod as well as on the insulating tube walls. An example of this result is shown in Figure 20 where, prior to the quartz probe pressurization, fuel leaked into the probe space and "coked" there. The problem was alleviated by pressurizing the quartz probe, but the purged probes had to be cleaned repeatedly, especially after DF-2 runs with high equivalence ratios. "Coked" fuel and soot deposition was almost negligible for JP-4.

The probes proved to be reasonably rugged, during this phase of the research. With carefull handling, the latest design probe (Figure 9) was operated at average temperatures of 800°C to 1100°C and transients of 1300°C, remaining intact after more than 2 hours of cumulative testing.

Cleaning the soot and coked fuel deposits with borax soap and toothpaste proved most effective.

4.2.3 Combustion Efficiency

4.2.3.1 Thermal combustion efficiency was determined by dividing the combustor thermal energy output by the fuel's net heat of combustion. As might be expected, the design fuel, JP-4, was the most efficient, and DF-2 exhibited the lowest baseline efficiency. Comparison of consecutive tests for

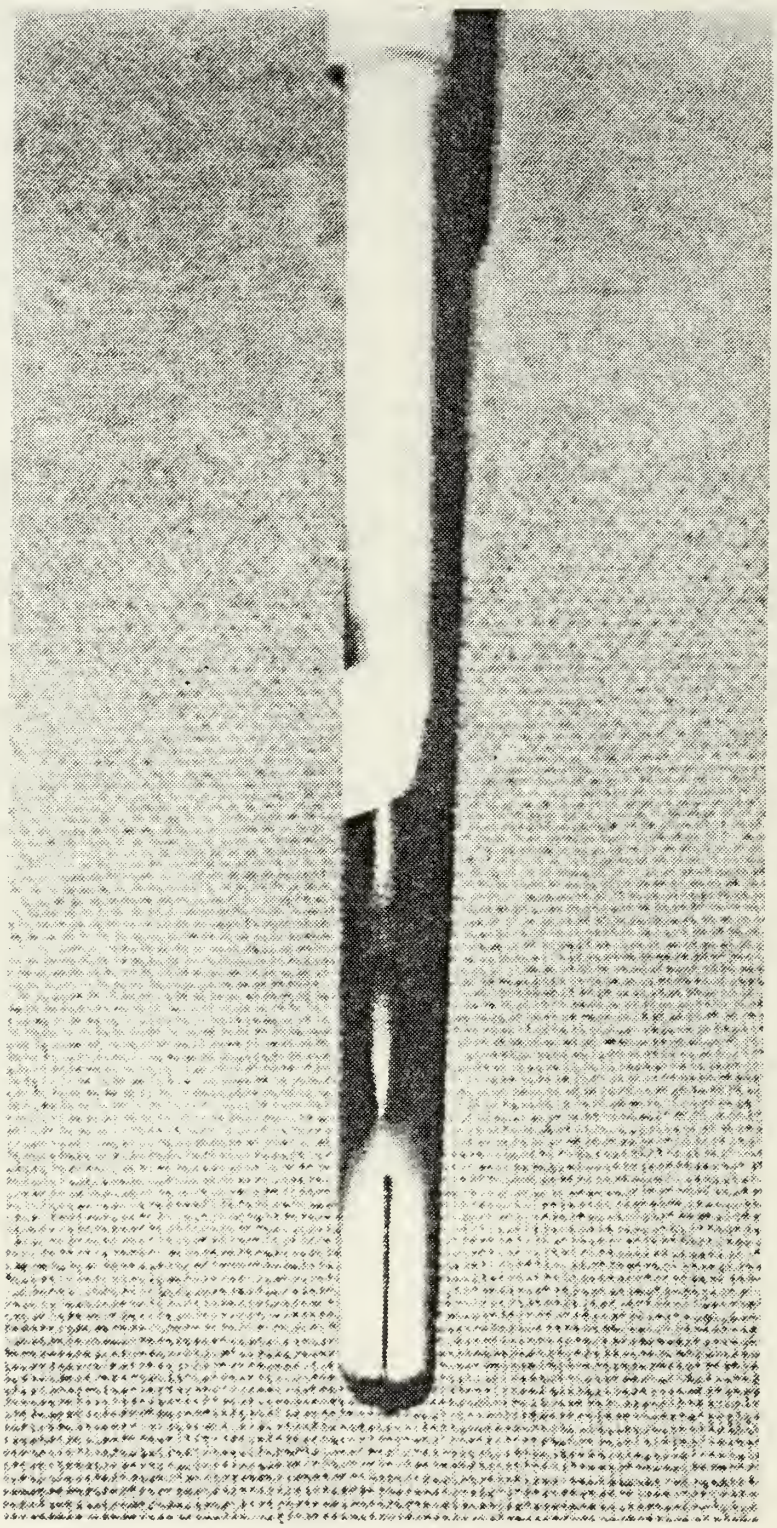

FIG. 19 TYPICAL PROBE SOOT DEPOSITION PATTERN

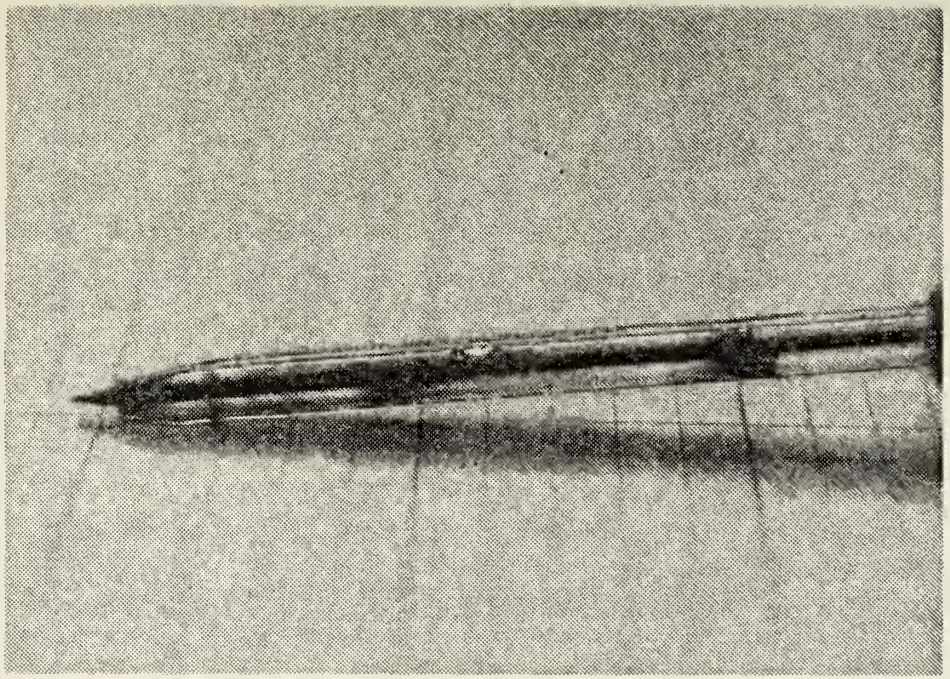

FIG. 20 PROBE DETAIL SHOWING INTERNAL SOOT DEPOSITS

JP-4 and DF-2, with the same electrode configuration at zero potential is given in Figure 21. The thermal combustion efficiency η is in the vicinity of 90 percent, that of DF-2 being lower than that of JP-4 by about five percent.

4.2.3.2 Changes in thermal combustion efficiency are equivalent to the relative net combustion temperature rise:

$$\frac{\Delta T}{T}$$

An average exhaust temperature change indicative of increased combustion efficiency was detected for all fuels with the application of high voltage to the electrode. A summary of Tests Results is given in table 4.2.* There is a trend for greater improvement, and over a wider range of combustion conditions and electrode configurations, for the higher viscosity and higher surface tension fuels.

It can be seen that for each electrode configuration there was only a narrow range of ER for each fuel in which an increase in exhaust temperature could be achieved. This is believed to be due to the difficulty maintaining high electical fields with the variations in the flamefront position for various fuels and ERs.

For practical applications, the most important results are those achieved with ER < 1.

Due to limitations of the air supply, the combustor was operated at low pressures and temperatures, which would be representative of very high altitudes (usually above the operation ceiling for T-56 engines).

It should be noted, that for ER < 1 , the improvements in η for small gap distances were achieved mostly with very low electrical currents, indicating

*Temperature and voltage recordings for JET-A, JP-5, and DF-2 tests are presented in Figures 22a, b, and c, respectively.

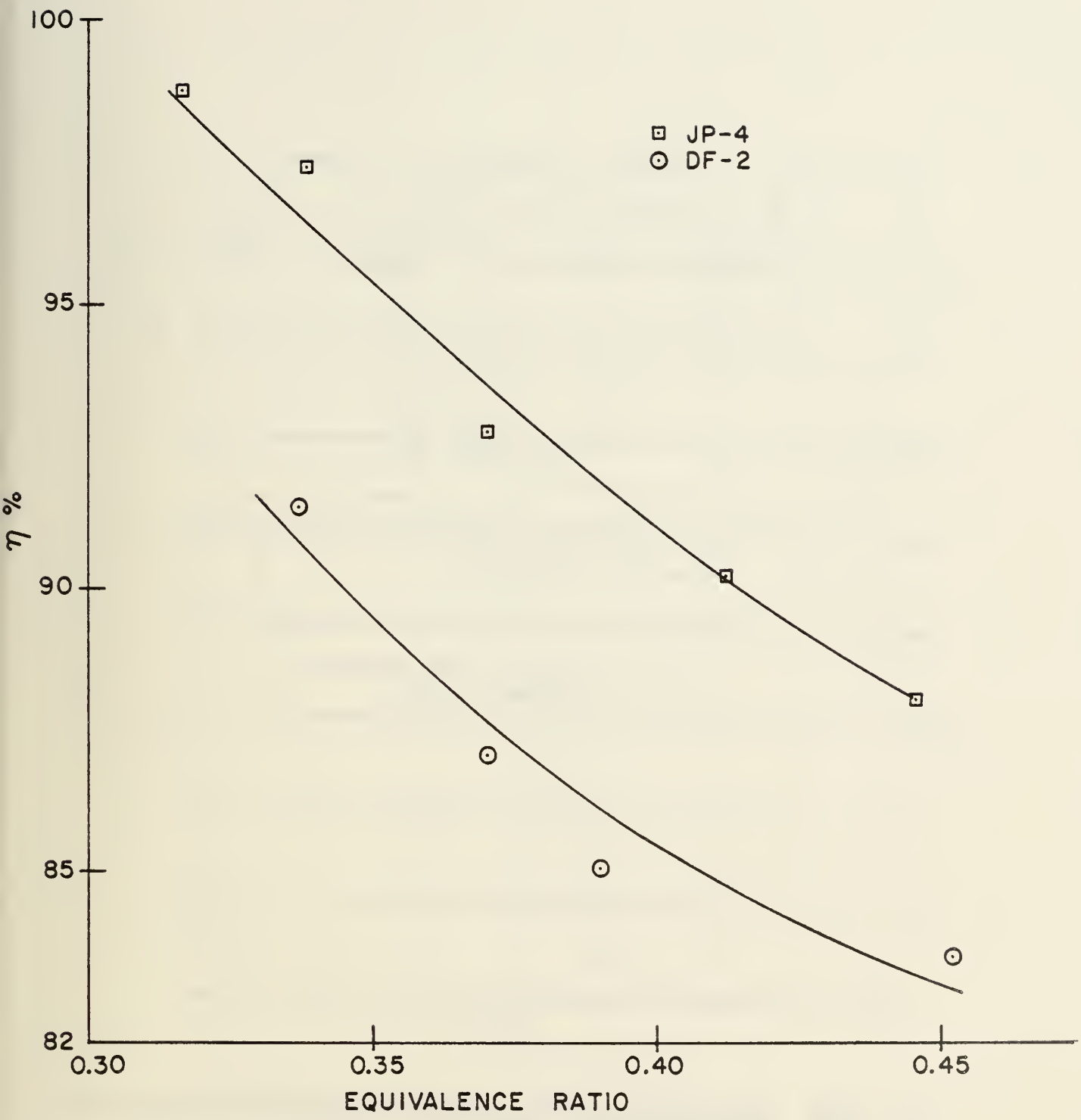

FIG. 21 COMPARISON OF THERMAL COMBUSTION EFFICIENCY BETWEEN JP-4 AND DF-2, PROBE AT ZERO POTENTIAL

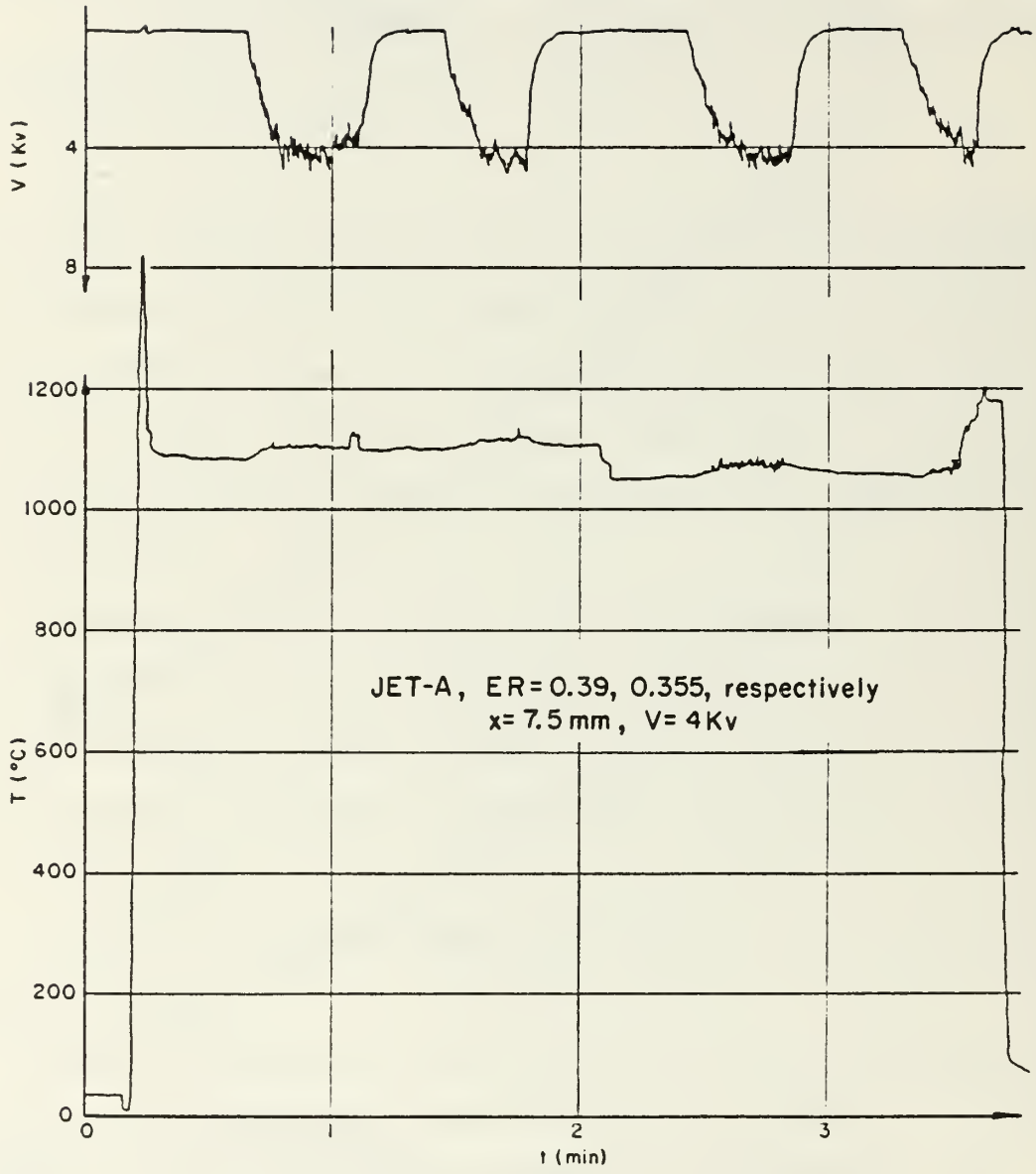

FIG. 22a TEMPERATURE-VOLTAGE RECORDING JET-A

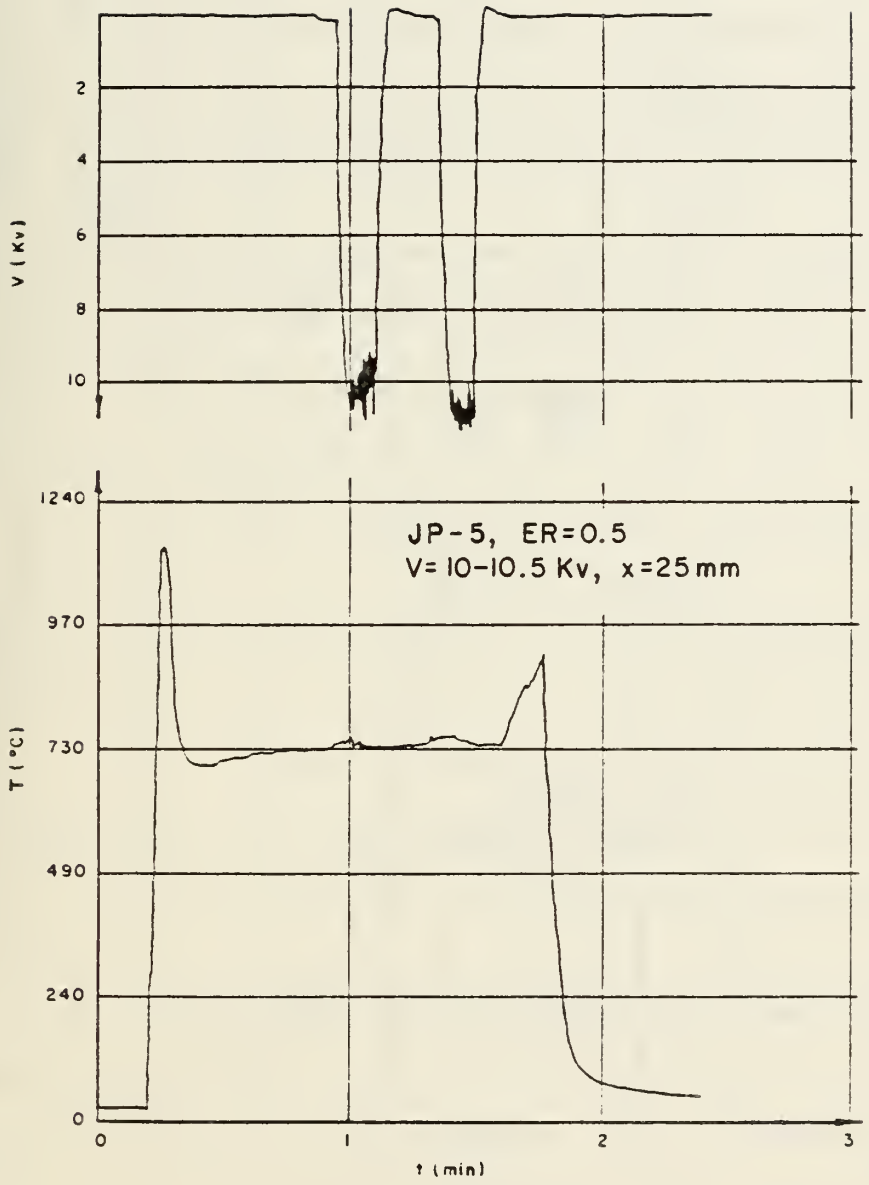

FIG. 22b TEMPERATURE—VOLTAGE RECORDING JP-5

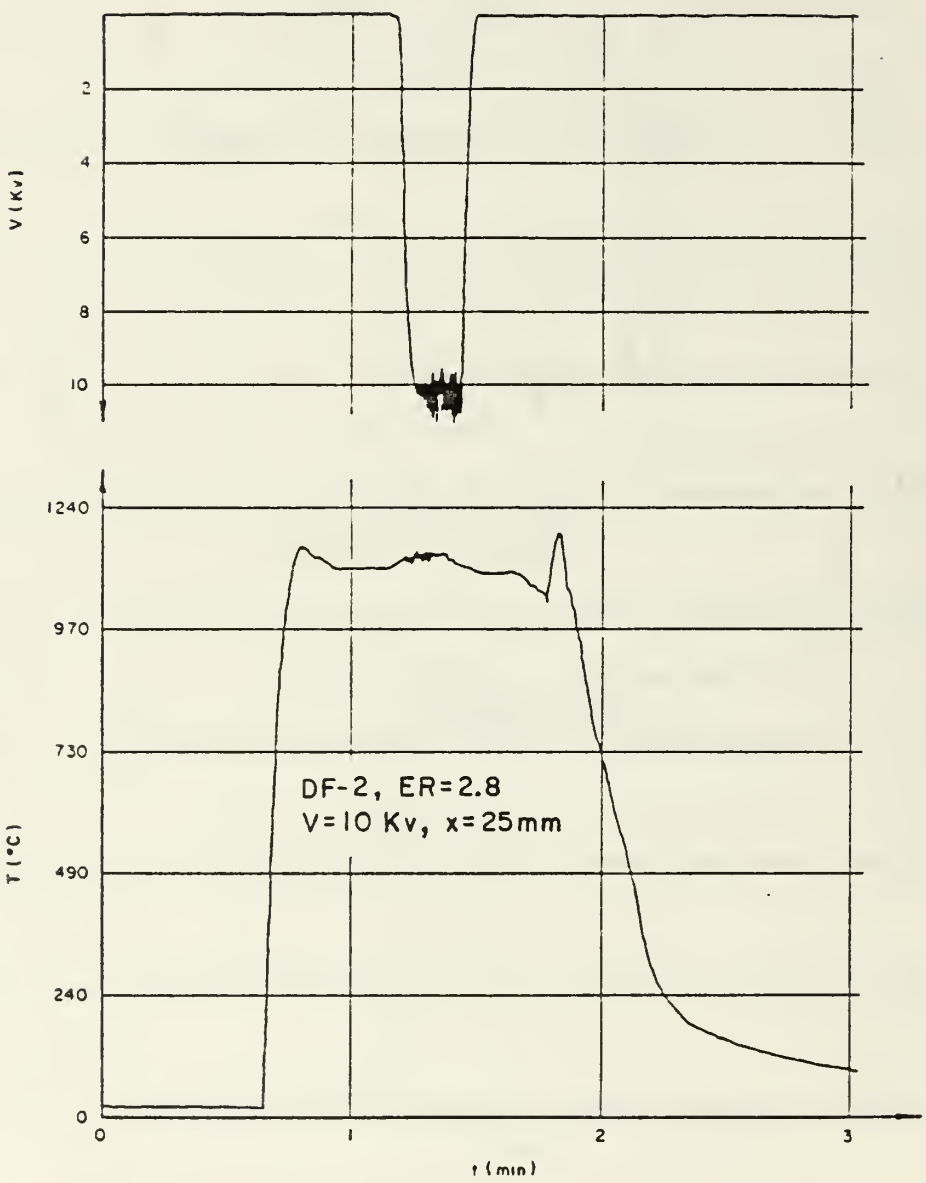

FIG. 22c TEMPERATURE–VOLTAGE RECORDING DF-2

TABLE 2

Summary Test Results

Test #	Fuel	ER	$V_{(kV)}$	$I_{(mA)}$	X(mm) gap distance	T (°C)	Δn	Remarks
4-21-7	JET A(2)	0.38	~4		7.5	923	+0.3%	Sharp point, sealed probe
4-21-10	JET A	0.36	4+		7.5	845	+0.6%	
4-21-11	JET A	0.392	4.6	low	7.5	922	0.4%	
4-21-12	JET A	0.355	4.6	low	7.5	858	1.0%	
4-21-13	JP-4(2)	0.402	4.4	low	7.5	942	0.6%	
4-21-14	JP-4	0.362	4.0	low	7.5	877	0.35%	
5-17-18	JP-4	0.38	8.0	4.5	20	900	0.55%	Blunt, double insulated purged probe
5-17-19	JP-4	0.345	8.0	4.5	20	836	0.48%	
5-18-2	JP-4	0.345	9.0	5	25	826	0.6%	
5-20-1	JP-4	0.395	10.0	4.5	35	900	0.44%	
5-20-2	JP-4	0.358	9.0	4.5	35	855	0.6%	

TABLE 2 CONTINUED

Summary Test Results

Test #	Fuel	ER	V(kV)	I(mA)	X(mm) gap distance	T (°C)	Δη	Remarks
5-13-11	DF-2(2)	2.44	4.0	5	9-10	1113		Blunt, double insulated purged probe
5-17-12	DF-2	0.452	8.0	1-2	15	968	0.4%	
5-17-13	DF-2	0.39	8.0	1÷2	15	850	1.06%	
5-17-14	DF-2	0.37	8.0	1÷2	15	836	0.5%	
5-17-26	DF-2	0.363	8.0	4.5	20	843	0.6%	
5-18-10	DF-2	0.396	9.0	4.5	25	883	+	
5-20-14	DF-2	0.38	4;6;7	<0.2	7.5	883	0.9%	
10-29-10	DF-2(1)	2.8	10,10.3	5	25	1150	3%;1.6%	Sharp point,purged probe
10-29-11	DF-2	2.8	10	5	25	1150	2.4%; 3.6%	

TABLE 2 CONTINUED

Summary Test Results

Test #	Fuel	ER	V(kV)	I(mA)	X(mm) gap distance	T (°C)	Δη	Remarks
11-2-2	DF-2	3.08	10.5	5	25	1150	3%	Sharp point, purged probe Based on "K" central only
11-2-3	DF-2	3.45	10.0	5	25	1100	3%	$\frac{\Delta T}{T}$
11-2-4	DF-2	4.27	10.9	5	25	1050	3.5%	$\frac{\Delta T}{T}$
11-2-6	JP-5(1)	2.94	11.4	5	25	1188	0.7%	$\frac{\Delta T}{T}$
11-2-7	JP-5	4.4	11.4	5	25	1010	0.8%	$\frac{\Delta T}{T}$
11-2-8	JP-5	0.475	10.3	5	25	790	2.1%	TC probably a little outside

TABLE 2 CONTINUED

Summary Test Results

Test #	Fuel	ER	$V_{(kV)}$	$I_{(mA)}$	X(mm) gap distance	T (°C)	Δn	Remarks
11-4-1	JP-5(1)	0.417	10.5	5	25	760	1.7%	Sharp point, purged probe Based on "K" central only Probe deterioration
11-4-2	JP-5	0.415	10.8	5	25	760	1%	
11-4-3	JP-5	0.419	10.3	5	25	775	0.7%	
11-4-8	JET A(1)	0.467	10.0	5	25	809	1.5%	
11-4-11	JET A	0.53	10.0	5	25	955	0.6%	
11-4-12	JET A	2.86	10.2	5	25	1090	2.4%	$\frac{\Delta T}{T}$
11-5-1	JET A	3.3	11.1	5	25	1120	1.1%	$\frac{\Delta T}{T}$
11-5-2	JET A	3.35	10.8	5	25	1090	1.2%	$\frac{\Delta T}{T}$

(1) Batch used through December 1982
(2) Batch used through January - September 1983

predominantly electrostatic charging, while for larger gaps the discharge current was greater, indicating electrohydrodynamic charging.

It is worth observing that, even for the highest values of voltage and current recorded, the input electrical power is of the order of 1 percent of the gains achieved in the thermal output power.

4.2.3.3 In most tests changes in the exhaust temperature profile were detected with high voltage application, even if the sum-averaged temperature remained constant or with insignificant positive changes. This indicates spray-pattern distortions due to the forces between the charged droplets and the high voltage electrode. Normally there was an increase in the exhaust temperature profile on the side of the electrode.

4.2.3.4 In no case was a negative average temperature change detected with high voltage application.

5. LIGHT ABSORPTION AND SCATTERING EXPERIMENTS

5.1 Most of the cold-spray experiments were conducted with JET-A. The number of fuels was restricted to avoid fuel ignition hazard. The output signal of the lock-in amplifier contained fluctuations, indicating temporal changes in spray pattern. The average value of this signal was reasonably constant and repeatable. This average value was taken as the measure of light transmission through the spray.

During the control tests a rectified signal from the reference detector was recorded indicating a constant laser output power, (laser manufacturer's specifications are: ripple < 0.5%, power variations in 8 hours < ±5%).

5.2 Both blunt and pointed grounded electrodes were tested, with the nozzle at a high negative potential. The electrodes tested were both of the right angle and nozzle centerline type. The best D_{32} reduction was obtained with the right angle blunt electrode having a gap distance of about 8.5 mm. This is consistent with the results of combustion tests, where the best results for JET-A were achieved for x ≅ 7.5 mm. The transmission dropped from 0.39 to 0.375, indicating a decrease of 4 percent in D_{32} (Figure 23). Correction of this value for slight changes in ℓ and C_v , caused by the mutual repulsion of like charged droplets, and recorded photographically, (Figure 24), yields a relative D_{32} change of between 6.7 and 7.7 percent.

In comparison with this result, the change in the "most probable droplet diameter" obtained by Kelly [9] with the more sophisticated "spray triode," was about 20 percent. Ito et al., [7] found that applying high voltages with a ring electrode near the fuel nozzle improved fuel atomization and decreased the droplet mean diameter and standard deviation.

5.3 Absolute SMD was measured for DF-2 on the setup described in Section 3.2.3. The pinhole was moved through θ = 0.926, θ = 1.852 and θ = 2.78 mrad.

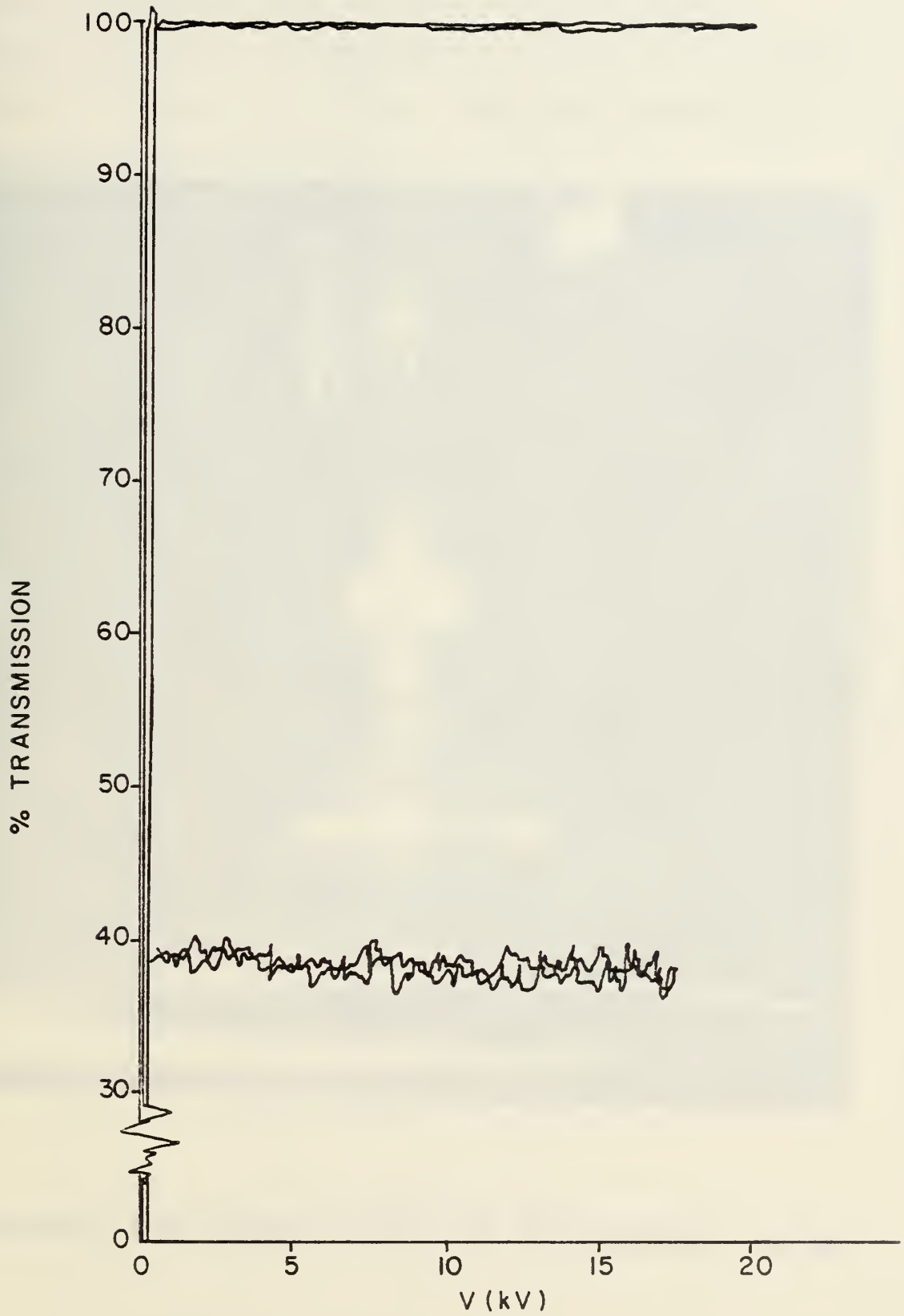

FIG. 23 PERCENT TRANSMISSION vs APPLIED POTENTIAL FOR A 10mm GAP IN JET A

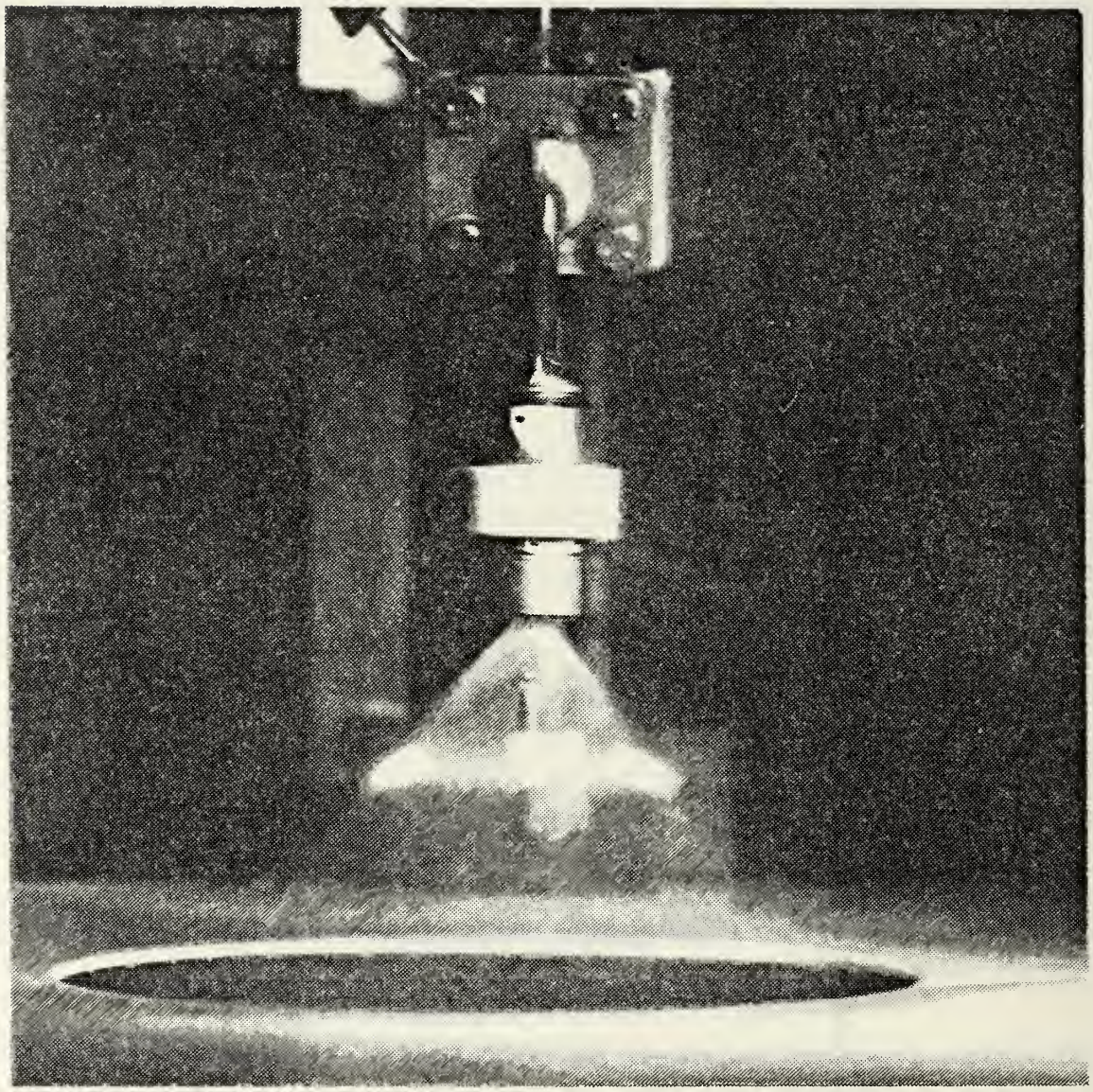

FIG. 24 PHOTOGRAPH OF LIGHT ABSORPTION EXPERIMENT

The measured values of $I(\theta)$ were repeatable to within 25 percent in consecutive tests. D_{32} was calculated according to the curves in [16,23], yielding the values $217\mu m > D_{32} > 201\mu m$. Calculation according to [24] (equation (3.6)) yielded $D_{32} = 207\mu m$.

6. CONCLUSIONS

6.1 General

While full scale development of electrohydrodynamic fuel spray enhancement would be best conducted in an industrial facility, numerous goals can and should be pursued on the existing experimental setups. These include both cold spray diagnostics and verification in combustion experiments.

6.2 Improved Electrode Design

Higher electrical fields can be achieved at the nozzle utilizing a ring-mesh ("flyswatter") electrode. This is indicated by the values of electrical field with point-(or sphere)-to-plane electrodes vs. rod-to-plane configurations (Reference [25]). This configuration would probably result in stronger flameholding and consequently would entail additional or enhanced flame holder reduction strategies.

6.3 Insulated-Nozzle Combustion Tests

The problem of flame holding and the resulting presence of conducting gases can be alleviated by insulating the nozzle in the combustor can, charging it with high negative potential and keeping the electrode grounded (see Figure 25). Based on the results of the unpurged quartz-insulated probe, there are no conductive gases in the neighborhood of the nozzle (within about 7.5 mm), thus high voltages may be applied to the nozzle with very low leakage currents. As the flame front is at ground potential, flameholding on the grounded electrode would pose no problem. The electrode, however, would have to be protected against oxidation and high temperature. Moreover, it could be incorporated in the combustor liner as a rigid fixture.

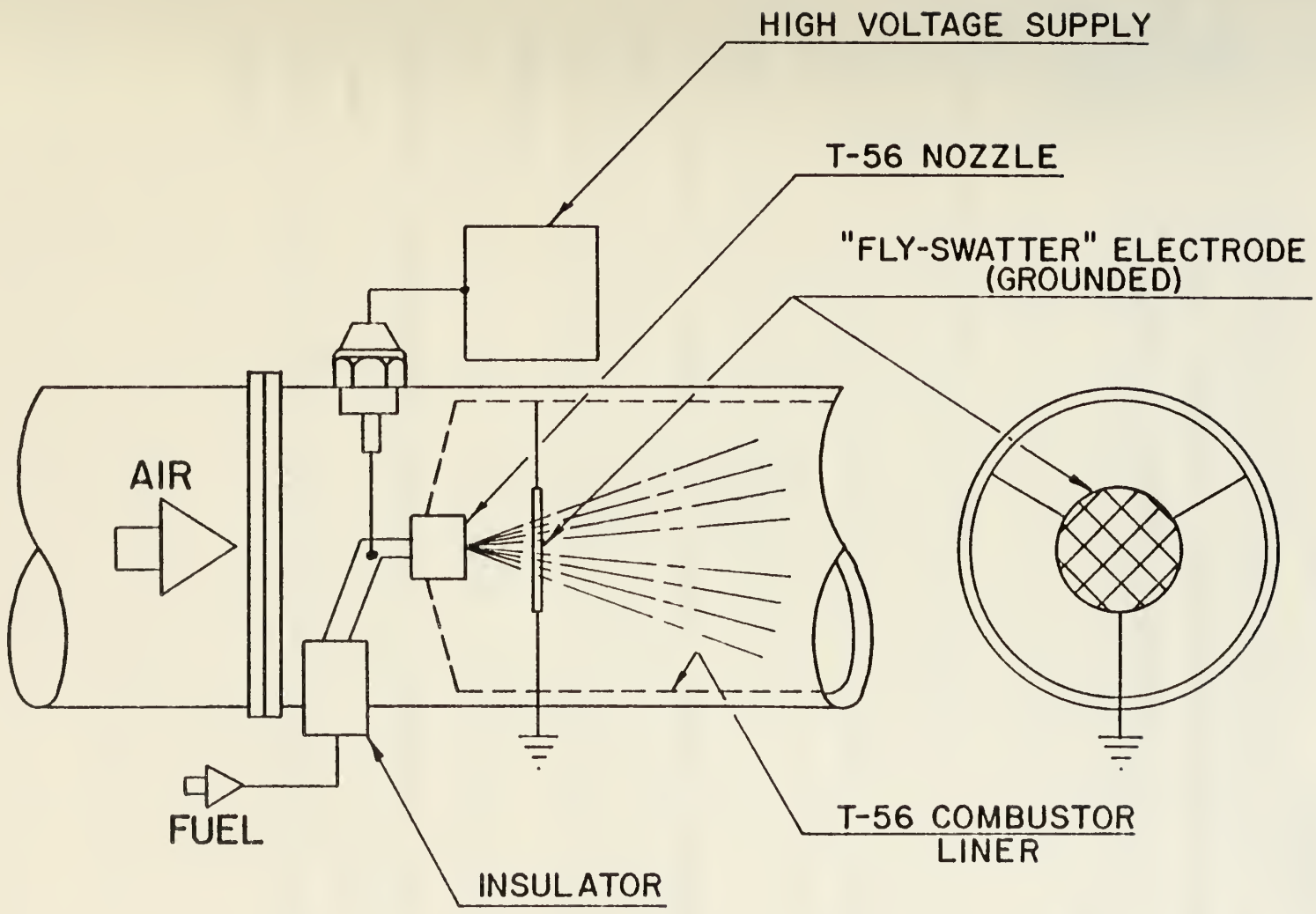

FIG. 25 INSULATED NOZZLE / GROUNDED ELECTRODE

6.4 SMD Measurement

The photodiode array at the focal plane can be utilized for $I(\theta)$ measurements, eliminating the need for micrometric screw adjustments during the tests. Two angle measurements along with the high voltage can be recorded on a 3-channel recorder yielding sufficient data for D_{32}-vs-V calculations [24].

7. SUMMARY

7.1 An existing combustion test rig has been modified and an optical scattering experiment designed and constructed for the continuation of the research on the electrohydrodynamic enhancement of fuel sprays for gas turbines.

7.2 Optical absorbtion tests indicate a Sauter Mean Diameter decrease with the application of electrical fields.

7.3 Combustion efficiency in a real-size combustor, a modified T-56 can, was improved with the application of high electrical fields, up to 0.6% for JP-4, 1% for JET-A, 3.6% for DF-2, and 2.1% for JP-5, for equivalence ratios between 0.35 and 0.53, and voltages between 4 kV and 11kV.

7.4 These results, achieved with nonoptimal electrode configurations, indicate the potential for significant combustion and propulsion efficiency improvements, with perhaps relatively minor retrofit needs in existing combustors.

7.5 A "side-effect" detected during this study, the distortion of combustor temperature distribution may be the basis of an additional combustor design parameter. This could result in greater flexibility in combustor design, and possibly to lowering of the liner temperature, extending the combustor's lifetime.

REFERENCES

1. "Aircraft Engine Future Fuels and Energy Conservation," Agard Lecture Series No. 96, September 1978.

2. J .P. Longwell,"Combustion of Liquid Fuels" in Combustion Processes, B. Lewis, R.N. Pease, H.S. Taylor, Editors, Princeton University Press, 1956.

3. A. H. Lefevre, Gas Turbine Combustor Design Problems, Hemisphere Publishing Co., 1980.

4. A. M. Kanury, Indroduction to Combustion Phenomena, Gordon and Breach Science Publishers, 1975.

5. "Evaluation of Fuel Character Effects on JP79 Smokeless Combustor," AFWAL-TR-80-2092, ESL-TR-80-46, November 1980.

6. L. W. L. Rayleigh, The Theory of Sound, Dover, 1945.

7. K. Ito, K. Yamane, and S. Fukazawa, "Electrostatic Atomization of Liquid Fuels," Journal of the Fuel Society of Japan, v. 51, pp. 724-732, September 1972, [In Japanese].

8. A. J. Kelly, "Electrostatic Spray Theory," Journal of Applied Physics, Vol. 49, No. 5, May 1978, pp. 2621 - 1628.

9. A. J. Kelly, "The Electrostatic Atomization of Hydrocarbons," 2nd International Conference on Liquid Atomization and Spray Systems, Madison, WI, June 20-15, 1982.

10. L. L. Todd, "Design of an Apparatus for the Study of Electrostatic Effects on Gas Combustor Efficiency," Masters Thesis, Naval Postgraduate School, Monterey, California, September 1981.

11. R. J. Laib, "Design of an Apparatus for the Study of Electrohydrodynamic Control of Spray from Fuel Injectors in Gas Turbines," Engineer's Thesis, Naval Postgraduate School, Monterey, California, December 1982.

12. J. M. Logan, "Electrohydrodynamic Spraying of Aviation Fuels in a Gas Turbine," Masters Thesis, Naval Postgraduate School, Monterey, California, June 1982.

13. J.A. Mavroudis, "Experimental Study of Electrostatically Modified Fuel Sprays on Gas Turbine combustor Performance," Masters Thesis, Naval Postgraduate School, Monterey, California, December 1982.

14. "Flow Measurement," American Society of Mechanical Engineers Publication, 1959.

15. W.W. Manning, "Study of Electrostatic Modulation of Fuel Sprays to Enhance Combustion Performance in an Aviation Turbine," Master's Thesis, Naval Postgraduate School, Monterey, California, in Press.

16. R.A. Dobbins, L. Crocco, I. Glassman, "Measurement of Mean Particle Sizes of Sprays from Diffractively Scattered Light," AIAA Journal, Vol. 1, No. 8, p. 1882, August 1963.

17. A.A. Rizkalla and A.H. Lefevre, "The Influence of Air and Liquid Properties on Airblast Atomization," Journal of Fluids Engineering, p. 316, September 1975.

18. K.L. Cashdollar, C.K. Lee, J.M. Singer, "Three-Wavelength Light Transmission Technique to Measure Smoke Particle Size and Concentration," Applied Optics, Vol. 18, No. 11, p. 1763, June 1974.

19. W.D. Bachalo, D.F. Hess and C.A. Hartwell, "An Instrument for Spray Droplet Size and Velocity Measurements," Engineering for Power, Vol. 102, No. 4, October 1980.

20. H.C. van de Hulst, Light Scattering by Small Particles, John Wiley & Sons, Inc., New York, NY, 1957.

21. R.B. Penndorf, "An Approximation to the Mie Theory for Colloidal Spheres," Journal of Physics and Chemistry, Vol. 62, p. 1537, December 1958.

22. M. Born and E. Wolf, Optics, Pergamon Press Oxford, 1975.

23. J.H. Roberts and M.J. Webb, "Measurement of Droplet Size for Wide Range Particle Distributions," AIAA Journal, Vol. 2, No. 3, p. 583, March 1964.

24. D.R. Buchele, "Particle Sizing by Measurement of Forward-Scattered Light at Two Angles," NASA Technical Paper 2156, 1983.

25. J.M. Mattingley and H.M. Ryan, "Standard and Practical Electrode Systems," Proceedings of the IEEE, Vol. 118, No. 5, p. 720, May 1971.

26. Energy Management Laboratory, Turbine Fuel Test Reports 82-F-2025/2026/2027, October 1982 and 83-F-0541/0542/0543, March 1983, Wright-Patterson Air Force Base.

27. R.F. Stearns, R.R. Johnson, R.M. Jackson, and C.A. Larson, Flow Measurement With Orifice Meters, D. Van Nostrand, New York, 1951.

APPENDIX A

THE ELECTRIC INJECTOR

Combustor design is complicated by droplet atomization which in turn depends not only on the fuel but also on the fluid mechanics of the injector region. Future burner designs will no doubt benefit from new concepts on atomization which focus on the characteristics of electrified droplets. The range of droplet size modulation which has been demonstrated by electrostatic means can be extended to encompass a more substantial electrical role. Examples of such injectors are to be found in ink-jet printing devices[A1-A4] and in the coherent injector program[A5] at Edwards Air Force Base.

At the heart of these new electric injectors is a fuel manifold/nozzle combination in which piezoelectric crystal synchronization produces drops which are substantially more uniform than present injectors which rely only on fluid mechanical forces. In the ink-jet printer droplet size uniformity is of paramount importance and atomization is accomplished over relatively small distances when compared to gas turbine injectors. Moreover, in the printer, droplets at each miniature jet have to be individually addressable with relatively high precision. In a burner, more room should be available if only to keep the flame away from the injector region, and droplets have to be charged not as much for addressability (depending, of course, on the geometries involved) but for fine tuning or control of different fuel properties. Clearly, with the new "degrees of freedom" available, new design concepts will evolve.

The coherent injector derives its name from the potential coherence of the fuel spray. The full advantages in combustion devices of a uniform size droplet with controllable spatial penetration has yet to be assessed but it appears likely that much more compact and versatile devices will evolve.

Needless to say, with truly coherent injectors, combustion theory will benefit and hopefully simplify.

To date, the electric injector effort seems to be in its infancy and only the Edwards effort has been identified. We must, therefore, look primarily at the ink-jet printer for practical guidance in the developmental problems that lie ahead.

APPENDIX A

REFERENCES

A1. L. Kuhn and R. A. Myers, "Ink-Jet Printing," Scientific American, Volume 240, No. 4, pp. 162, April 1979.

A2. R. G. Sweet, "High Frequency Recording with Electrostatically Deflected Ink," Review of Scientific Instruments, Volume 36, No. 2, pp. 131, February 1965.

A3. R. H. Hein and D. E. Lundquist, "Synchronous Jet Ink Droplet Generator Mechanism," SID International Symposium Digest of Technology Papers, pp. 212, San Diego, California, April 1980.

A4. R. D. Carnaban and S. L. Hou, "Ink Jet Printing Devices," IEEE Conference Record of IAS Conferences Meeting, pp. 10, Atlanta, Georgia, September-October 1975.

A5. Private Communication with Mr. Kurt Selph, AFRPL, Edwards Air Force Base, California--Project Directive, Project 5730055V, "Liquid Rocket Motor Coherent Injector Study," Part I-Project Engineering.

INITIAL DISTRIBUTION LIST

		No. Copies
1.	Defense Technical Information Center Cameron Station Alexandria, Virginia 22314	2
2.	Library, Code 0142 Naval Postgraduate School Monterey, California 93943	2
3.	Department Chairman, Code 67 Department of Aeronautics Naval Postgraduate School Monterey, California 93943	1
4.	Associate Professor O. Biblarz, Code 67Bi Department of Aeronautics Naval Postgraduate School Monterey, California 93943	7
5.	Professor J. Miller, Code 67Mo Department of Aeronautics Naval Postgraduate School Monterey, California 93943	7
6.	Mr. A. Zajdman Visiting Research Associate Department of Aeronautics Naval Postgraduate School Monterey, California 93943	2
7.	Commanding Officer Naval Air Systems Command Attn: Mr. G. Derderian, Code AIR 330B Attn: Mr. Tom Momiyama, Code AIR 330 Washington DC 20361	10 1
8.	Dr. Alan Roberts Headquarters, Naval Material Command Energy and Natural Resources Research and Development Officer Navy Department Washington DC 20360	2
9.	Mr. C. D. B. Curry, Patent Counsel Office of Naval Research One Hallidie Plaza, Suite 601 San Francisco, California 94102	2

10. Dr. A. J. Kelly — 1
Department of Mechanical and Aerospace Engineering
Princeton University
Princeton, New Jersey 08544

11. Mr. J. Yount — 1
SA-ALC-SF TLA
Aerospace Fuels Laboratory
Building 70, Area B
Wright Patterson Air Force Base, Ohio 45433

12. Dr. R. S. Colladay — 1
Director, Research and Development
Technology Division
NASA Headquarters
Washington DC 20546

13. Mr. J. S. Grobman — 1
Chief, Fuels Technology Branch
NASA Lewis Research Center
21000 Brookpark Road
Cleveland, Ohio 44135

14. Mr. C. L. Delaney — 1
Airforce Aero Propulsion Laboratory
Wright Patterson Air Force Base, Ohio 45433

15. Mr. R. A. Rudey — 1
NASA Lewis Research Center
2100 Brookpark Road
Cleveland, Ohio 44135

16. Mr. N. F. Rekos — 1
Office of Aeronautics and Space Technology
NASA Headquarters
Washington DC 20546